

1        **Rain evaporation, snow melt and entrainment at the**  
2        **heart of water vapor isotopic variations in the tropical**  
3        **troposphere, according to large-eddy simulations and a**  
4        **two-column model**

5                    **Camille Risi <sup>1</sup>, Caroline Muller <sup>1</sup>, Peter Blossey <sup>2</sup>**

6        <sup>1</sup>Laboratoire de Meteorologie Dynamique, IPSL, CNRS, Ecole Normale Supérieure, Sorbonne Université,

7                    PSL Research University, Paris, France

8        <sup>2</sup>Department of Atmospheric Sciences, University of Washington, Seattle, USA

9        **Key Points:**

- 10        • Isotopic enrichment of tropospheric water vapor by rain evaporation is stronger  
11        when drier air enhances sublimation and evaporation  
12        • Entrainment of dry air weakens the vertical isotopic gradient and limits the de-  
13        pletion of tropospheric water vapor.  
14        • These mechanisms explain the increased depletion of tropospheric water vapor as  
15        tropospheric relative humidity increases.

---

Corresponding author: Camille RISI, [crlmd@lmd.jussieu.fr](mailto:crlmd@lmd.jussieu.fr)

## 16 Abstract

17 The goal of this study is twofold. First, we aim at developing a simple model as  
 18 an interpretative framework for the water vapor isotopic variations in the tropical tropo-  
 19 sphere over the ocean. We use large-eddy simulations to justify the underlying assump-  
 20 tions of this simple model, to constrain its input parameters and to evaluate its results.  
 21 Second, we aim at interpreting the depletion of the water vapor isotopic composition in  
 22 the lower and mid-troposphere as precipitation increases, which is a salient feature in  
 23 tropical oceanic observations. This feature constitutes a stringent test on the relevance  
 24 of our interpretative framework. Previous studies, based on observations or on models  
 25 with parameterized convection, have highlighted the roles of deep convective and meso-  
 26 scale downdrafts, rain evaporation, rain-vapor diffusive exchanges and mixing processes.

27 The interpretative framework that we develop is a two-column model represent-  
 28 ing the net ascent in clouds and the net descent in the environment. We show that the  
 29 mechanisms for depleting the troposphere when precipitation rate increases all stem from  
 30 the higher tropospheric relative humidity. First, when the relative humidity is larger, less  
 31 snow sublimates before melting and a smaller fraction of rain evaporates. Both effects  
 32 lead to more depleted rain evaporation and eventually more depleted water vapor. This  
 33 mechanism dominates in regimes of large-scale ascent. Second, the entrainment of dry  
 34 air into clouds reduces the vertical isotopic gradient and limits the depletion of tropo-  
 35 spheric water vapor. This mechanism dominates in regimes of large-scale descent.

## 36 Plain Language Summary

37 Water molecules can be light (one oxygen atom and two hydrogen atoms) or heavy  
 38 (one hydrogen atom is replaced by a deuterium atom). These different molecules are called  
 39 water isotopes, and their relative concentration in water is called the isotopic composi-  
 40 tion. The isotopic composition of the precipitation recorded in ice cores or in speleothems  
 41 can be used to reconstruct past climates. However, the factors controlling the isotopic  
 42 composition are complex. Here we aim at developing a simple model as an interpreta-  
 43 tive framework for the water vapor isotopic variations in the tropical troposphere over  
 44 the ocean. As a guide for developing this framework, we use high-resolution atmospheric  
 45 simulations that explicitly simulates vertical motions in the storms. As a test for this  
 46 framework, we try and interpret why in observations, the precipitation and water vapor  
 47 are more depleted when storm activity is stronger. We find that stronger storm activ-  
 48 ity, when associated with stronger large-scale ascent, is associated with a moister tro-  
 49 posphere. This reduces the sublimation of snow, the fraction of rain that evaporates and  
 50 the dilution of cloudy air by entrainment, ultimately leading to more depleted water va-  
 51 por and precipitation.

## 52 1 Introduction

### 53 1.1 Looking for an interpretative framework for water vapor isotopic 54 profiles

55 The isotopic composition of water vapor (e.g. its Deuterium content, commonly  
 56 expressed as  $\delta D = (R/R_{SMOW} - 1) \times 1000$  in ‰, where  $R$  is the ratio of Deuterium  
 57 over Hydrogen atoms in the water, and SMOW is the Standard Mean Ocean Water refer-  
 58 ence) evolves along the water cycle as phase changes are associated with isotopic frac-  
 59 tionation. Consequently the isotopic composition of precipitation recorded in paleocli-  
 60 mate archives has significantly contributed to the reconstruction of past hydrological changes  
 61 (Wang et al., 2001). It has also been suggested that observed isotopic composition of wa-  
 62 ter vapor could help better understand atmospheric processes and evaluate their repre-  
 63 sentation in climate models, in particular convective processes (Schmidt et al., 2005; Bony

64 et al., 2008; Lee et al., 2009; Field et al., 2014). Yet, water isotopes remain rarely used  
 65 beyond the isotopic community to answer today’s pressing climate questions. A prereq-  
 66 uisite to better assess the strengths and weaknesses of the isotopic tool is to better un-  
 67 derstand what controls spatio-temporal variations in water vapor isotopic composition  
 68 ( $\delta D_v$ ) through the tropical troposphere, and in particular how convective processes drive  
 69 these variations.

70 While there are interpretative frameworks for the controls of free tropospheric hu-  
 71 midity (Sherwood, 1996; Romps, 2014), no such interpretative framework exist for wa-  
 72 ter isotopes beyond the simple Rayleigh distillation or mixing lines (Worden et al., 2007;  
 73 Bailey et al., 2017). We aim at filling this gap here. The first goal of this paper is thus  
 74 to design an interpretative framework that could be useful in the future to interpret wa-  
 75 ter vapor isotopic variations in the tropical troposphere in a wide range of contexts. Anal-  
 76 ogous to that for relative humidity, this framework will also allow us to compare the pro-  
 77 cesses controlling relative humidity and isotopic composition.

78 Frameworks do exist to interpret the  $\delta D_v$  in the sub-cloud layer (SCL), such as the  
 79 Merlivat and Jouzel (1979) closure assumption, later extended to account for mixing with  
 80 free tropospheric air (Benetti et al., 2015) and for updrafts and downdrafts (Risi et al.,  
 81 2020). This latter framework highlighted the need to know the steepness of the relation-  
 82 ship between  $\delta D_v$  and specific humidity  $q$  as they evolve with altitude. This motivates  
 83 us to develop a framework that allows us to predict the  $\delta D_v$  evolution with altitude in  
 84 the troposphere.

## 85 **1.2 Large-eddy simulation analysis as a guide to design the interpreta-** 86 **tive framework**

87 Many previous studies investigating the processes controlling tropospheric  $\delta D_v$  have  
 88 relied on general circulation models that include convective parameterization (Lee et al.,  
 89 2007; Bony et al., 2008; Risi et al., 2008; Field et al., 2010). However, parameterizations  
 90 include numerous simplifications or assumptions that are responsible for a significant part  
 91 of biases in the present climate simulated by GCMs and of inter-model spread in climate  
 92 change projections (Randall et al., 2003; Stevens & Bony, 2013; Webb et al., 2015). Here,  
 93 we thus use large-eddy simulations (LES) as a guide to design the interpretative frame-  
 94 work. These high-resolution simulations allows us to explicitly resolve convective mo-  
 95 tions. These simulations will also provide the input parameters for our interpretative frame-  
 96 work, and a benchmark to evaluate its results.

## 97 **1.3 Interpreting the amount effect**

98 In the tropics, it has long been observed that in average over a month or longer,  
 99 the isotopic composition of the rain is more depleted when the precipitation rate is stronger  
 100 (Dansgaard, 1964; Rozanski et al., 1993). This phenomenon is called the “amount ef-  
 101 fect”. Since most of the precipitation in the tropics is associated with deep convection,  
 102 understanding the amount effect is a stringent test on our understanding of how convec-  
 103 tive processes affect the water isotopic composition in the tropical troposphere. The ca-  
 104 pacity of our interpretative framework to predict the amount effect will thus be a strin-  
 105 gent test on its relevance. The second goal of this study is thus to better understand the  
 106 processes underlying the amount effect, using the interpretative framework.

107 Dansgaard (1964) hypothesized that the amount effect could be due to the progres-  
 108 sive depletion by convective storms of the vapor from which the rain forms, and to rain  
 109 evaporation and diffusive exchanges between the rain and the vapor. If the case, the amount  
 110 effect crucially depends on the isotopic composition of the vapor. From a column-integrated  
 111 water budget perspective, the isotopic composition of precipitation depends on the rel-  
 112 ative proportion of the precipitation that originates from horizontal advection and from

113 surface evaporation (Lee et al., 2007; Moore et al., 2014). More precipitation is gener-  
 114 ally associated with more large-scale ascent and thus more large-scale convergence. Since  
 115 vapor from horizontal advection is more depleted than water from surface evaporation  
 116 because it has already been processed in clouds, the precipitation is more depleted. In  
 117 this view as well, the amount effect crucially depends on the isotopic composition of the  
 118 vapor.

119 Water isotopic measurements in the vapor phase, by satellite or in-situ, have con-  
 120 firmed that increased precipitation was associated with more depleted water vapor (Worden  
 121 et al., 2007; Kurita, 2013; Lacour et al., 2017). Hereafter we will call this the “vapor amount  
 122 effect”. Actually, the precipitation and water vapor isotopic composition often vary in  
 123 concert (Kurita, 2013; Tremoy et al., 2014). In this paper, we will thus focus on under-  
 124 standing the processes underlying the “vapor amount effect”.

125 From previous studies, four hypotheses have emerged to explain the “vapor amount  
 126 effect”:

- 127 1. Hypothesis 1: As precipitation rate increases, convective or meso-scale downdrafts  
 128 bring more depleted vapor from above into the sub-cloud layer (SCL) (Risi et al.,  
 129 2008; Kurita et al., 2011; Kurita, 2013). This is because  $\delta D_v$  generally decreases  
 130 with altitude, because as water vapor is lost through condensation and  $q$  decreases,  
 131 heavy isotopes are preferentially lost in the condensed phase. This phenomenon  
 132 is called Rayleigh distillation and is plotted in a  $q-\delta D_v$  diagram in Figure 1 (blue).  
 133 However, downdrafts would both decrease  $\delta D_v$  and  $q$ . This hypothesis is thus in-  
 134 consistent with the observation that  $q$  generally increases while  $\delta D_v$  decreases as  
 135 precipitation rate increases. By itself, this hypothesis cannot be sufficient.
- 136 2. Hypothesis 2: As precipitation rate increases, the moistening effect by rain evap-  
 137 oration increases. If rain evaporation is more depleted than the vapor, then it de-  
 138 pletes the vapor (Worden et al., 2007). The effect of rain evaporation is represented  
 139 in purple in Figure 1. If the evaporated fraction of the rain is small, rain evapo-  
 140 ration acts to deplete the vapor because light isotopes preferentially evaporate.
- 141 3. Hypothesis 3: As precipitation rate increases, the rain evaporation is more depleted.  
 142 For example, if precipitation rate increases, the fraction of rain that evaporates  
 143 is smaller. Because heavy isotopes diffuse through air more slowly than  $H_2^{16}O$ , the  
 144 initial vapor produced by rain evaporation is more depleted than the average iso-  
 145 topic composition of the rain. As a larger fraction of the raindrop evaporates, the  
 146 vapor produced by evaporation becomes less depleted and can sometimes be more  
 147 enriched than the surrounding vapor (Risi et al., 2008, 2010; Tremoy et al., 2014;  
 148 Risi et al., 2020) (Figure 1, purple). Alternatively, larger precipitation rates typ-  
 149 ically occur in moister environments, which favors rain-vapor diffusive exchanges  
 150 rather than pure evaporation (Lawrence et al., 2004; Lee & Fung, 2008). Since rain  
 151 comes from higher altitudes, it is more depleted than if in equilibrium with the  
 152 local vapor, and thus rain-vapor diffusive exchanges favor more depleted evapo-  
 153 ration.
- 154 4. Hypothesis 4: As precipitation rate decreases, dehydration by mixing dominates  
 155 relatively to dehydration by condensation. Due to the hyperbolic shape of the mix-  
 156 ing lines in a  $q-\delta D$  diagram, dehydration by mixing with a dry source is asso-  
 157 ciated with a smaller depletion than predicted by Rayleigh distillation (Dessler  
 158 & Sherwood, 2003; Galewsky & Hurley, 2010; Galewsky & Rabanus, 2016) (Fig-  
 159 ure 1 orange). Bailey et al. (2017) argues that in more subsiding regions, mid-tropospheric  
 160 vapor is more enriched for a given  $q$  because air masses result from the mixing be-  
 161 tween air subsiding from a higher altitude and shallow convective detrainment.

162 We notice that hypothesis 2-4 are all associated with an increased steepness as precip-  
 163 itation rate increases (Figure 1), consistent with the key role of the steepness of the  $q-$   
 164  $\delta D_v$  relationship in depleting the SCL water vapor highlighted by Risi et al. (2020). The

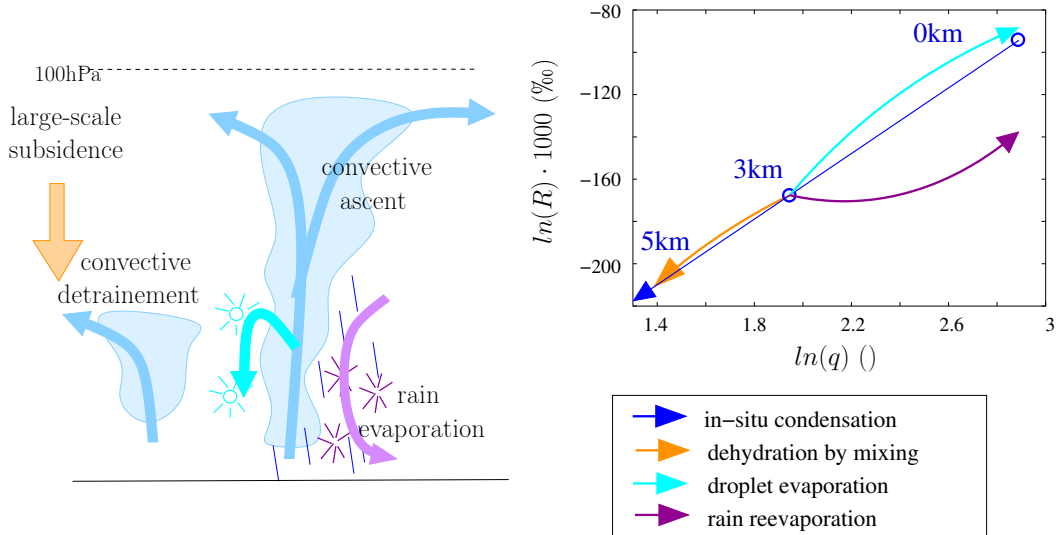


**Figure 1.** Schematic showing the influence of different processes on  $q$  and  $\delta D_v$ . Condensation and immediate loss of condensate in convective updrafts leads to drying and depleting the water vapor following Rayleigh distillation (blue). During evaporation of cloud droplets, each droplet evaporates totally. Since cloud droplets are enriched in heavy isotopes, this moistens the air and enriches the vapor (cyan). In contrast, during evaporation of rain drops, each drop evaporates progressively. Whereas it moistens the air, it depletes the vapor for small evaporation fractions and enriches the vapor for large evaporation fraction (purple). Finally, mixing of subsiding air with air detrained from convective updrafts dehydrates the air and depletes the vapor following a hyperbolic curve, leading to higher  $\delta D_v$  for a given  $q$  compared to Rayleigh (orange). The curves are plotted following simple Rayleigh and mixing lines with approximate values taken from the control LES described later in the article.

165 mechanisms underlying these hypotheses will thus have to be key ingredients of our inter-  
 166 prepretative framework.

167 The LES will be described and analyzed in section 2. The interpretative framework  
 168 will be designed and used to interpret the “vapor amount effect” in section 3. Finally,  
 169 section 4 will offer a summary, some discussion and perspectives.

## 170 2 Large-eddy simulations

### 171 2.1 Model and simulations

172 We use the same LES model as in Risi et al. (2020), namely the System for Atmo-  
 173 spheric Modeling (SAM) non-hydrostatic model (M. F. Khairoutdinov & Randall, 2003),  
 174 version 6.10.9, which is enabled with water isotopes (Blossey et al., 2010). This model  
 175 solves anelastic conservation equations for momentum, mass, energy and water, which  
 176 is present in the model under six phases: water vapor, cloud liquid, cloud ice, precipi-  
 177 tating liquid, precipitating snow, and precipitating graupel. We use the bulk, mixed-phase  
 178 microphysical parameterization from Thompson et al. (2008) in which water isotopes were  
 179 implemented (Moore et al., 2016).

180 The control simulation (“ctrl”) is three-dimensional, with a doubly-periodic domain  
 181 of 96 km×96 km. The horizontal resolution is 750 m. There are 96 vertical levels. The  
 182 simulation is run in radiative-convective equilibrium over an ocean surface. The sea sur-

183 face temperature (SST) is 30°C. There is no rotation and no diurnal cycle. In this sim-  
 184 ulation, there is no large-scale circulation.

185 The amount effect can be seen only if the precipitation increase is associated with  
 186 a change in the large-scale circulation (Bony et al., 2008; Dee et al., 2018; Risi et al., 2020).  
 187 To compare ctrl to simulations with larger and smaller precipitation rate, we thus run  
 188 simulations with a prescribed large-scale vertical velocity profile,  $\omega_{LS}$ . This profile is used  
 189 to compute large-scale tendencies in temperature, humidity and water vapor isotopic com-  
 190 position. We compute large-scale vertical advection by a simple upstream scheme (Godunov,  
 191 1959). In the computation, large-scale horizontal gradients in temperature, humidity and  
 192 isotopic composition are neglected, i.e. there are no large-scale horizontal advective forc-  
 193 ing terms. The large-scale vertical velocity  $\omega_{LS}$  has a cubic shape so as to reach its max-  
 194 imum  $\omega_{LSmax}$  at a pressure  $p_{max}=500$  hPa and to smoothly reach 0 at the surface and  
 195 at 100 hPa (Bony et al., 2008). We analyze here simulations with  $\omega_{LSmax}=-60$  hPa/d  
 196 (“HighPrec”), corresponding to typical deep convective conditions in the inter-tropical  
 197 convergence zone, and  $\omega_{LSmax}=+20$  hPa/d (“LowPrec”), corresponding to subsiding trade-  
 198 wind conditions. The mean precipitation rates are 1.5, 2.5 and 8.5 mm/d respectively  
 199 in LowPrec, ctrl and HighPrec.

200 The simulations are run for 50 days and the last 10 days are analyzed. We use in-  
 201 stantaneous outputs that are generated at the end of each simulation day.

## 202 2.2 Simulated amount effect and basic features

203 Figure 2a shows that the ctrl, HighPrec and LowPrec simulations allow us to cap-  
 204 ture the amount effect both in the near-surface vapor and in the precipitation, which vary  
 205 in concert. In HighPrec, the domain-mean relative humidity  $h$  is larger than in ctrl by  
 206 more than 10% (Figure 2b), while  $\delta D_v$  is more depleted by more than 50‰, in most of  
 207 the troposphere (Figure 2c). We can see that the  $\delta D_v$  difference at all altitudes is sim-  
 208 ilar to that in the SCL. This confirms that understanding what controls the SCL  $\delta D_v$   
 209 is key to understand what controls  $\delta D_v$  at all altitudes (Risi et al., 2020). This also ex-  
 210 plains why models that assume constant SCL  $\delta D_v$  show very little sensitivity to all kinds  
 211 of convective and microphysical processes (Duan et al., 2018). We can also see that Rayleigh  
 212 distillation alone (dashed line) is a poor predictor of  $\delta D_v$  profiles and of their sensitiv-  
 213 ity to large-scale circulation.

## 214 2.3 Steepness of the $q - \delta D_v$ relationship

215 With the goal of understanding the amount effect, as a first step Risi et al. (2020)  
 216 focused on understanding what controls the  $\delta D_v$  in the SCL, because the SCL ultimately  
 217 feeds the water vapor at all altitudes in the troposphere. They identified the key role of  
 218 the steepness of the  $q - \delta D_v$  relationship of vertical profiles in the lower troposphere.  
 219 This steepness determines the efficiency with which updrafts and downdrafts near the  
 220 SCL top deplete the SCL. To understand what controls  $\delta D_v$  in the SCL and thus ev-  
 221 erywhere in the troposphere, we thus need to understand what controls the steepness  
 222 of the  $q - \delta D_v$  relationship.

223 The vertical profiles of  $\ln(R_v)$  as a function of  $\ln(q)$  for each simulation show a nearly  
 224 linear relationship (Figure 2d), consistent with a Rayleigh-like distillation process (Fig-  
 225 ure 1). If the vertical profiles were dominated by mixing processes, as in hypothesis 4,  
 226 the relationship would look concave down (Bailey et al., 2017) (Figure 1 orange). Rather,  
 227 in HighPrec, the curve looks concave up near the melting level, consistent with an ef-  
 228 fect of rain evaporation (Figure 1 purple).

229 To better quantify the steepness of the  $q - \delta D_v$  relationship, we define the  $q - \delta D_v$   
 230 steepness  $\alpha_z$ , as the effective fractionation coefficient that would be needed in a distil-  
 231 lation to fit the simulated joint  $q - \delta D_v$  evolution (Risi et al., 2020):

$$\alpha_z = 1 + \frac{\ln(R_v(z)/R_v(z-dz))}{\ln(q(z)/q(z-dz))} \quad (1)$$

232 The steepness  $\alpha_z$  in the ctrl simulation is smaller than that predicted by Rayleigh  
 233 distillation, i.e.  $\alpha_z < \alpha_{eq}$ , especially at higher altitudes (Figure 2e) (section 3.2.2 will  
 234 demonstrate that it is due to entrainment). Just above the SCL top,  $\alpha_z - 1$  is more than  
 235 three times larger in HighPrec than in ctrl. The increased steepness leads the updrafts  
 236 and downdrafts to deplete more efficiently the SCL water vapor (Risi et al., 2020), and  
 237 eventually the full tropospheric profile through mixing by deep convection. Conversely,  
 238 in LowPrec, the steepness is smaller and responsible for more enriched SCL. Our inter-  
 239 pretative framework will allow us to interpret these features (section 3).

#### 240 **2.4 Effect of de-activating rain-vapor exchanges**

241 According to hypotheses 2 and 3, the isotopic composition of the rain plays a key  
 242 role in the “vapor amount effect”. At a given instant and for a small increment of rain  
 243 evaporation fraction, the isotopic composition of the evaporation flux  $R_{ev}$  is simulated  
 244 following Craig and Gordon (1965):

$$R_{ev} = \frac{R_r/\alpha_{eq} - h_{ev} \cdot R_v}{\alpha_K \cdot (1 - h_{ev})}$$

245 where  $R_r$  and  $R_v$  are the isotopic ratios in the liquid water and water vapor,  $\alpha_{eq}$   
 246 and  $\alpha_K$  are the equilibrium and kinetic fractionation coefficient and  $h_{ev}$  is the relative  
 247 humidity. In order to test hypotheses 2 and 3, we run additional simulations similar to  
 248 ctrl and HighPrec but without any fractionation during rain evaporation, named “nofrac”,  
 249 where  $R_{ev} = R_r$ . We also run additional simulations with fractionation during evap-  
 250 oration, but with rain-vapor diffusive exchanges de-activated, named “nodiff”, where  $R_{ev} =$   
 251  $R_r/\alpha_{eq}/\alpha_K$ .

252 When fractionation during rain evaporation is de-activated,  $\delta D_v$  is more enriched,  
 253 consistent with a more enriched composition of rain evaporation (Figure 3a). In addi-  
 254 tion, the  $\delta D_v$  difference between HighPrec and ctrl is reduced by about 70% compared  
 255 to when all isotopic exchanges are considered (Figure 3c, red). This confirms that frac-  
 256 tionation during rain evaporation plays a key role in the “vapor amount effect”. When  
 257 rain-vapor diffusive exchanges are de-activated, the  $\delta D_v$  difference between HighPrec and  
 258 ctrl is reduced by about 30% compared to when all isotopic exchanges are considered (Fig-  
 259 ure 3c, green). Rain-vapor vapor diffusive exchanges thus play an important role as well.

260 We note that the  $\delta D_v$  difference between the simulations is remarkably constant  
 261 with altitude (Figure 3a,c), although we expect strong vertical variations in rain evap-  
 262 oration. This is consistent with the important role of the SCL  $\delta D_v$  as an initial condi-  
 263 tion for the full  $\delta D_v$  profile. We also note that more enriched  $\delta D_v$  profiles are associated  
 264 with a reduced lower-tropospheric steepness  $\alpha_z$  just above the SCL, and larger  $\delta D_v$  dif-  
 265 ferences between simulations are associated with larger differences in lower-tropospheric  
 266  $\alpha_z$ . This is consistent with the SCL  $\delta D_v$  being mainly driven by the steepness  $\alpha_z$  just  
 267 above the SCL (Risi et al., 2020). Finally, the reduced “vapor amount effect” in “nofrac”  
 268 leads to a reduced amount effect in the precipitation  $\delta D$  as well (Figure 3c, circles). This  
 269 shows that the column-integrated water budget (Lee et al., 2007; Moore et al., 2014) can-  
 270 not by itself predict the amount effect, since it depends on the isotopic composition of  
 271 the advected vapor, which can greatly vary depending on the detailed representation of  
 272 rain evaporation processes.

273 To summarize, in the total  $\delta D_v$  difference between HighPrec and ctrl, there is about  
 274 one third due to fractionation during evaporation, one third due to rain-vapor diffusive

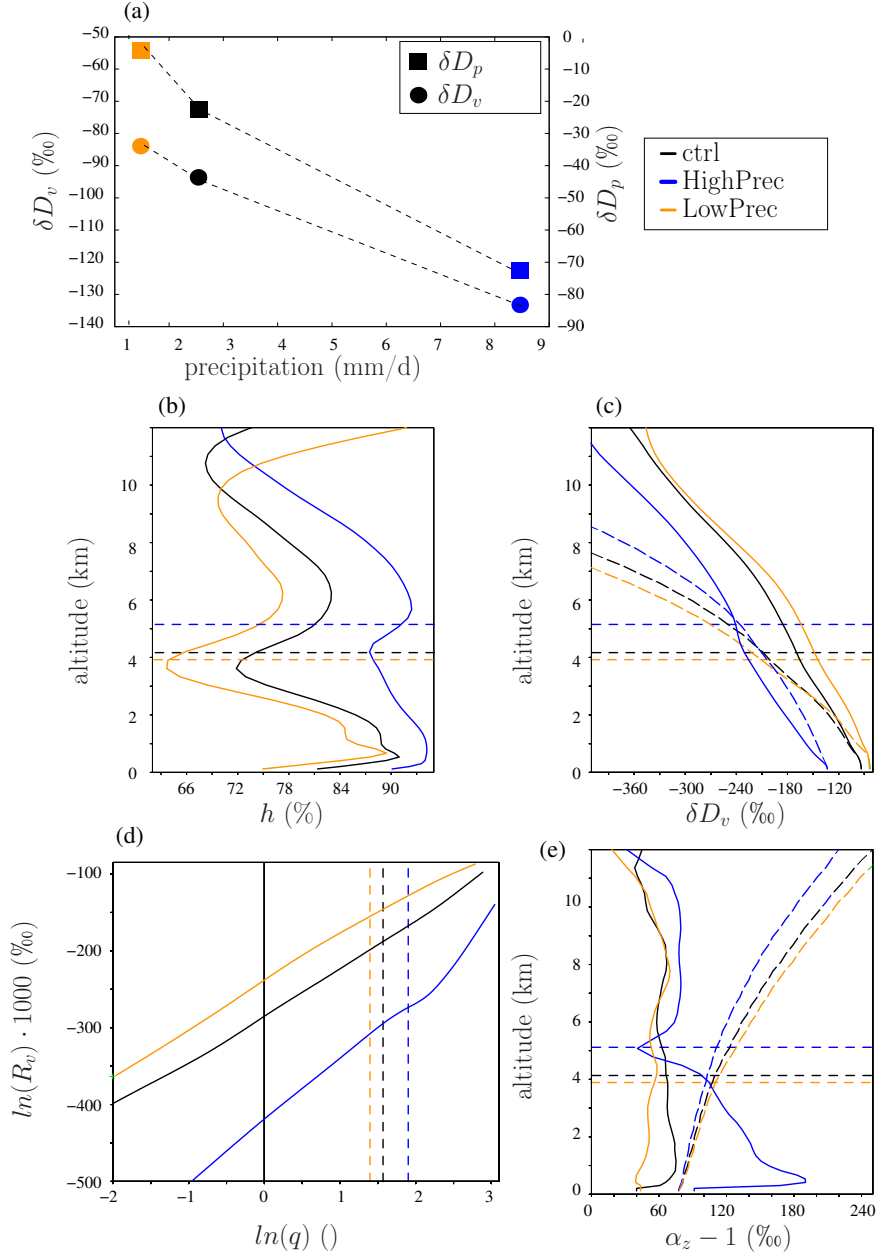


**Figure 2.** (a) Domain-mean water vapor (circles) and precipitation (squares)  $\delta D_v$  as a function of precipitation rate. Vertical distribution of relative humidity (b),  $\delta D_v$  (c) and  $\alpha_z$  (e) in ctrl (black), HighPrec (blue) and LowPrec (orange). (d)  $\ln(R_v(z)) \cdot 1000$  as a function of  $\ln(q(z))$  for different altitudes. In c and e, dashed lines indicate the prediction by Rayleigh distillation. The horizontal lines show the altitude of the melting level.

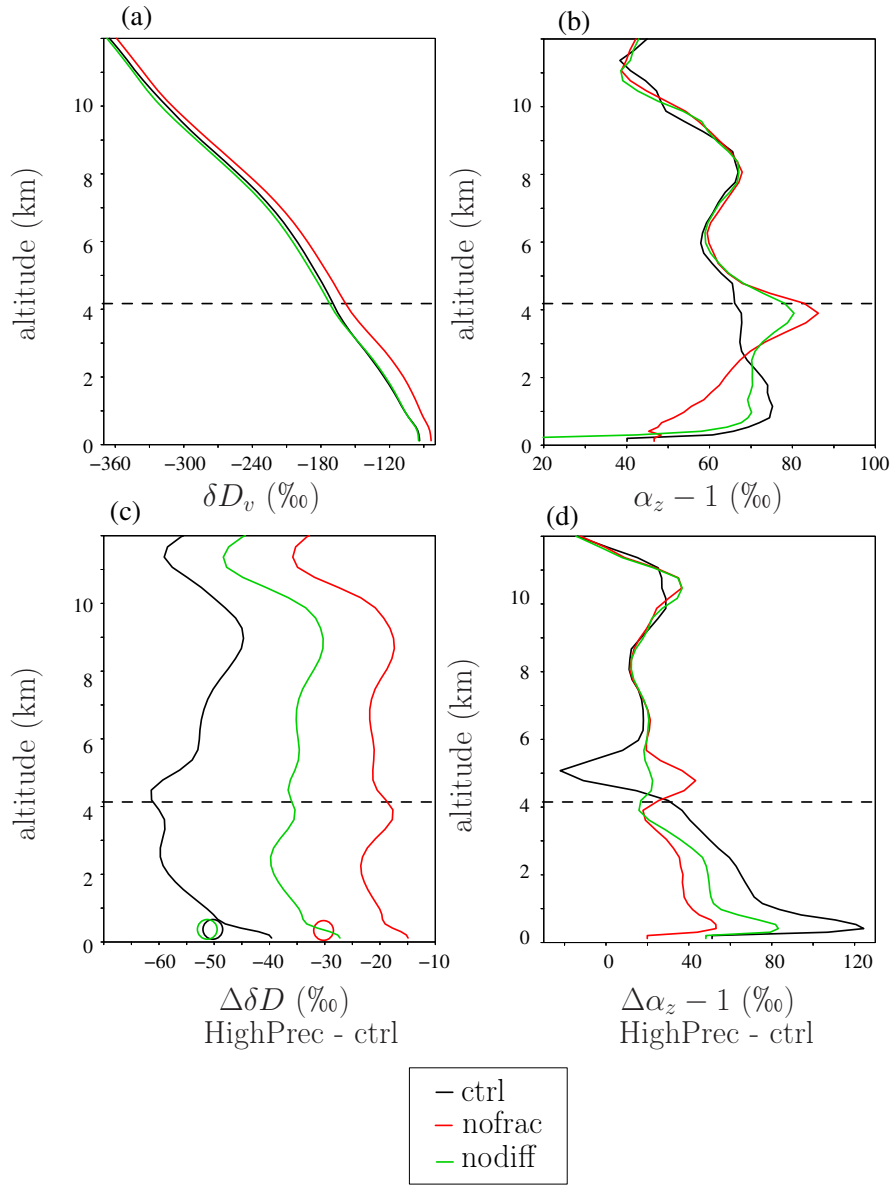


**Figure 3.** (a) Vertical distribution of  $\delta D_v$  for ctrl, when fractionation during liquid evaporation is turned on (black) or off (red) and when liquid-vapor equilibration is turned off (green). (b) Same as (a) for the vertical profiles of  $\alpha_z$ . (c)  $\delta D_v$  difference between the HighPrec and ctrl, with (black) and without (red) fractionation during evaporation and when liquid-vapor equilibration is turned off (green). The circles illustrate the difference in the precipitation  $\delta D$ . (d) Same as (c) but for  $\alpha_z$ .

275 exchanges, and one third that would remain even in absence of any fractionation dur-  
 276 ing evaporation. These tests suggest that hypotheses 2 and/or 3 play a key role in the  
 277 “vapor amount effect”. In the next sections, we aim at better understanding how rain  
 278 evaporation impacts  $\delta D_v$  profiles.

## 279 2.5 Vertical profiles binned by moist static energy

280 Previous studies have shown that analyzing variables in isentropic coordinates was  
 281 a powerful tool to categorize the different convective structures: undiluted updrafts, di-  
 282 luted updrafts, saturated and unsaturated downdrafts, and the environment (Kuang &  
 283 Bretherton, 2006; Pauluis & Mrowiec, 2013). This method also has the advantage of fil-  
 284 tering out gravity waves. It has been applied to the analysis of a wide range of convec-  
 285 tive systems (Mrowiec et al., 2015, 2016; Dauhut et al., 2017; Chen et al., 2018).

286 Here we use the frozen moist static energy  $m$  as a conserved variable because it is  
 287 conserved during condensation and evaporation of both liquid and ice water (C. J. Muller  
 288 & Romps, 2018; Hohenegger & Bretherton, 2011).

$$m = c_{pd} \cdot T + g \cdot z + L_v \cdot q_v - L_f \cdot q_i$$

289 where  $c_{pd}$  is the specific heat of dry air,  $T$  is temperature,  $g$  is gravity,  $z$  is altitude,  
 290  $L_v$  and  $L_f$  are the latent heat of vaporization and fusion, and  $q_i$  is the total ice water  
 291 content (cloud ice, graupel and snow). At each level, we categorize all grid points into  
 292 bins of  $m$  with a width of 0.4 kJ/kg.

293 The domain-mean  $m$  decreases from the upper troposphere down to about 5 km,  
 294 due to the loss of energy by radiative cooling, and then increases down to the surface due  
 295 to the input of energy by surface fluxes (Figure 4, solid black line). Based on this dia-  
 296 gram, we can identify four kinds of air parcels:

- 297 1. Environment. They correspond to air parcels whose  $m$  is close to the domain-mean  
 298 (solid black). They are the most numerous (Figure 4a). Their vertical velocity is  
 299 slightly descending (Figure 4b), but because they are very numerous, they account  
 300 for most of the downward mass flux (Figure 4c). Their relative humidity is close  
 301 to the domain-mean (Figure 4d), they contain only a small cloud water and rain  
 302 content and phase changes are very slow (Figure 4e-g). However, because they cover  
 303 most of the domain, they contribute significantly to the evaporation in the domain-  
 304 mean (Figure 4h).
- 305 2. Cloudy updrafts. They correspond to air parcels on the right of the domain-mean  
 306  $m$  and whose bin-mean vertical velocity is ascending (Figure 4b). If air rose adi-  
 307 abatically from the SCL, they would conserve their  $m$  and they would be located  
 308 completely on the right of the diagram. In practice,  $m$  decrease because the en-  
 309 vironment air is progressively entrained into ascending parcels. In the diagrams,  
 310 parcels are more diluted when they are closer to the domain-mean, and less di-  
 311 luted when they are more to the right. In spite of their dilution with the environ-  
 312 ment, their humidity is at saturation (Figure 4d). They contain a lot of cloud and  
 313 precipitating water, and vapor undergoes condensation (Figure 4e-g).
- 314 3. Cloudy downdrafts. They correspond to air parcels on the right of the domain-  
 315 mean  $m$  and whose bin-mean vertical velocity is descending (Figure 4b). They are  
 316 more diluted than cloudy updrafts. Their humidity is below saturation (Figure  
 317 4d). They contain cloud and precipitating water that undergo evaporation (Fig-  
 318 ure 4e-g). Located around the cloudy updrafts in the real space, they mainly cor-  
 319 respond to subsiding shells (e.g. Glenn and Krueger (2014)).
- 320 4. Precipitating downdrafts. They correspond to air parcels on the bottom-left of the  
 321 diagrams, with lower  $m$  relative to the domain-mean. They are among the most  
 322 strongly descending air parcels (Figure 4b) but since they are scarce (Figure 4b),

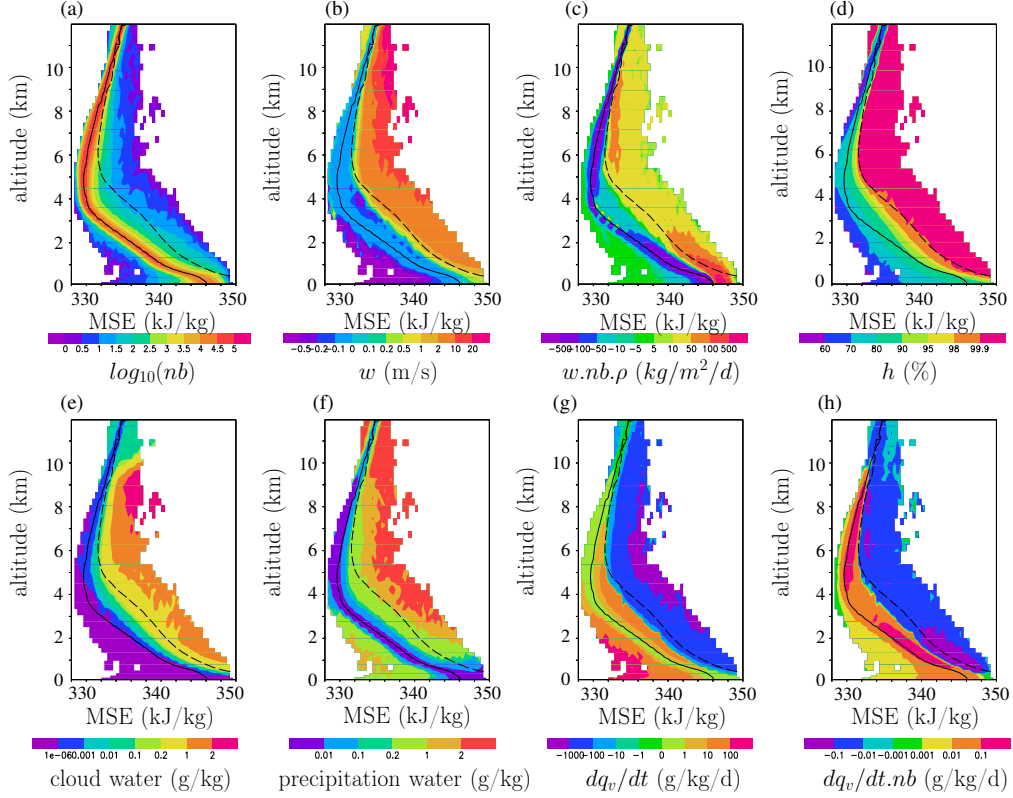


**Figure 4.** Variables binned as a function of frozen moist static energy  $m$  and of altitude, for the ctrl simulation: (a) number of samples, (b) vertical velocity anomaly, (c) vertical mass flux (vertical velocity multiplied by the proportion of samples and density), (d) relative humidity, (e) cloud water content mixing ratio (liquid and ice), (f) precipitating water mixing ratio (rain, graupel and snow), (g) evaporation and condensation tendency  $dq/dt$  (positive in case of evaporation, negative in case of condensation), (h)  $dq/dt$  multiplied by the number of samples. The solid black line show the domain-mean frozen moist static energy, while the dashed black line shows the frozen moist static energy at saturation.

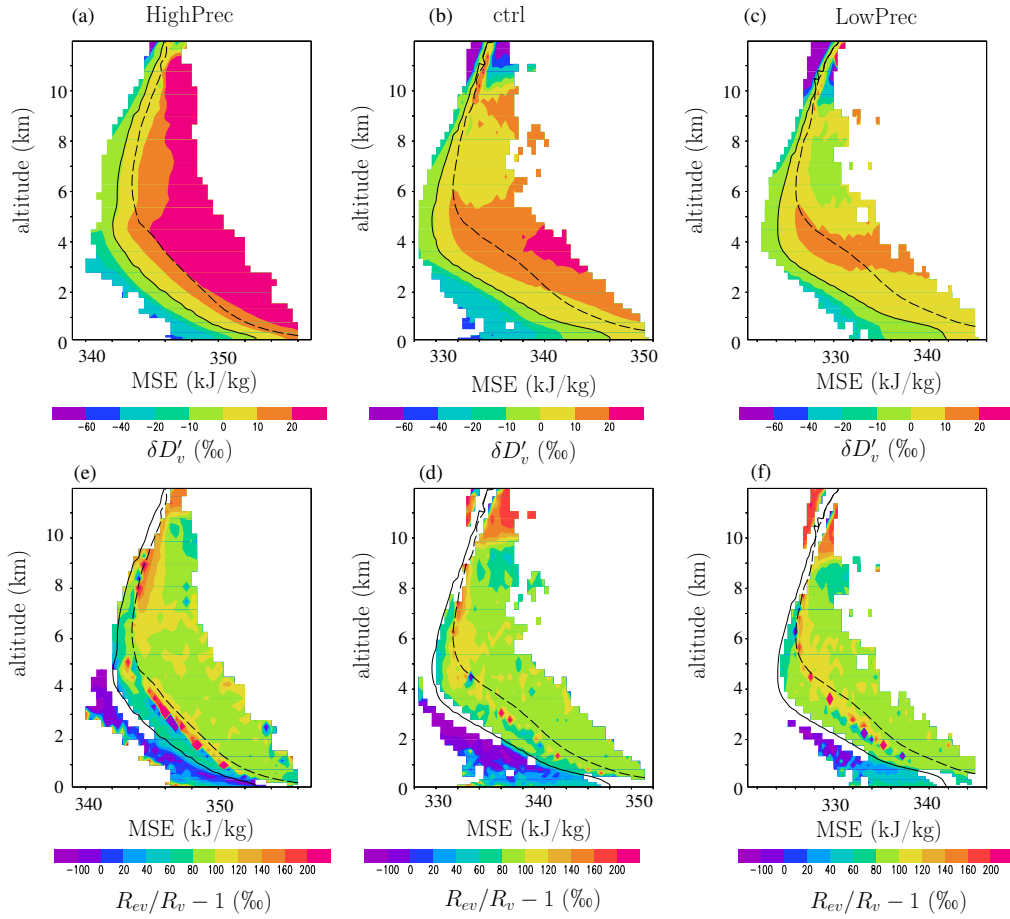


**Figure 5.** (b,e) As for Figure 4 but for (a)  $\delta D_v$  anomaly, (d)  $(\phi - 1) \cdot 1000$ , where  $\phi = R_{ev}/R_v$ ; it is expressed in ‰. (a,d) As for (b,e) but for HighPrec. (c,f) As for (b,e) but for LowPrec.

323 contribute little to the total descending mass flux (Figure 4c). They are very dry,  
 324 with no cloud water, but with precipitating water (Figure 4d-f). We interpret these  
 325 parcels as unsaturated, precipitating downdrafts. Strong evaporation of rain oc-  
 326 cur in these downdrafts (Figure 4g), but because they cover only a small fraction  
 327 of the domain, they contribute little to the evaporation in the domain-mean (Fig-  
 328 ure 4h).

329 The isotopic composition of water vapor is most enriched in the least diluted updrafts,  
 330 and most depleted in the precipitating downdrafts (Figure 5b). To assess the effect of  
 331 phase changes, we plot  $\phi = R_{ev}/R_v$ , where  $R_{ev}$  is the ratio of the water vapor tendency  
 332 associated with phase changes (evaporation in downdrafts and in the environment, or  
 333 condensation in cloudy updrafts) and  $R_v$  is the isotopic ratio of the water vapor in the  
 334 same  $m$ -altitude bin. In cloudy updrafts,  $\phi-1$  is about 100‰ in the lower troposphere  
 335 and increases with height (Figure 5e). This roughly corresponds to equilibrium fraction-  
 336 ation during condensation. In cloudy downdrafts,  $\phi-1$  is also about 100‰. This means  
 337 that cloud droplets evaporate totally without fractionation. In contrast, in precipitat-  
 338 ing downdrafts,  $\phi-1$  is much lower. It is around 30‰ below 1 km. The fact that  $\phi-1$   
 339 is positive is consistent with the fact that rain evaporation in the SCL acts to slightly  
 340 enrich the water vapor (Risi et al., 2020). In contrast, between 2 and 3 km,  $\phi-1$  is around  
 341 -100‰: at these levels, rain evaporation acts to deplete the water vapor, consistent with  
 342 Worden et al. (2007).

343 These diagrams look qualitatively similar for the other simulations. One notice-  
 344 able difference is that in HighPrec, the  $\delta D_v$  contrast between the environment and the  
 345 cloudy regions is larger (Figure 5a). This may be associated with the more depleted evap-  
 346 oration of the rain in precipitating downdrafts and of cloud droplets in cloudy downdrafts  
 347 (Figure 5d). Conversely in LowPrec, the  $\delta D_v$  contrast between the environment and the  
 348 cloudy regions is larger (Figure 5c). To quantitatively compare the different simulations,  
 349 now we plot vertical profiles of variables in average over cloudy regions and over the en-  
 350 vironment.

## 351 2.6 Vertical profiles for cloudy regions and for the environment

352 Here we chose to define cloudy regions as all parcels with a cloud (liquid or ice) wa-  
 353 ter content greater than  $10^{-6}$  g/kg (e.g. Thayer-Calder and Randall (2015)). In this loose  
 354 definition, “cloudy regions” correspond to both cloudy updrafts and downdrafts, while  
 355 the “environment” includes both the environment and precipitating downdrafts. Includ-  
 356 ing the cloudy downdrafts into the cloudy regions is justified by the fact that a signif-  
 357 icant portion of the water condensed in cloudy updrafts subsequently evaporate in these  
 358 cloudy downdrafts, without directly affecting the environment. Our results below are not  
 359 crucially sensitive to the definition of the cloudy regions and of the environment, pro-  
 360 vided that the definition of cloudy regions is not too restrictive (Text S1).

361 Cloudy regions cover only a few percent of the domain (Figure 6a). The fraction  
 362 of water condensed in cloudy regions that evaporates into the environment, estimated  
 363 as  $f_{ev} = -(dq/dt)_{env}/(dq/dt)_{cloud}$ , where  $(dq/dt)_{env}$  and  $(dq/dt)_{cloud}$  are the humid-  
 364 ity tendencies associated with phase changes in average in the environment and in the  
 365 cloudy region respectively, varies between 30% and 90%, depending on altitude (Figure  
 366 6b). It is smaller in HighPrec and than in ctrl, because the environment is moister.

367 Figure 6c plots  $\phi = R_{ev}/R_e$ , where  $R_{ev} = (dq_{HDO}/dt)_{env}/(dq/dt)_{env}$ ,  $(dq_{HDO}/dt)_{env}$   
 368 is the HDO tendency associated with phase changes in the environment and  $R_e$  is the  
 369 isotopic ratio in the environment. In all simulations except in HighPrec near 4.5 km,  $\phi >$   
 370 1: the evaporation has an enriching effect on the environment. The overall enriching ef-  
 371 fect of evaporation contradicts hypothesis 2. Yet in all cases,  $\phi < \alpha_{eq}$ : the evaporation  
 372 is not as enriching as if there was total evaporation of condensate. The  $\phi$  is smaller in

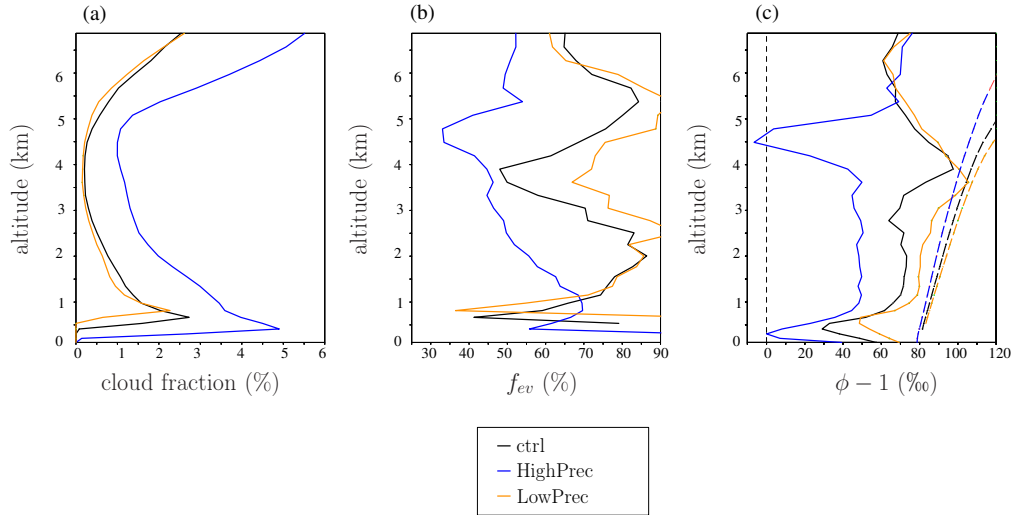


**Figure 6.** (a) fraction of the domain covered by cloudy regions. (b) Fraction of the water condensed in cloudy regions that evaporates into the environment,  $f_{ev}$ . (c)  $(\phi - 1) \cdot 1000$  (solid) and  $(\alpha_{eq} - 1) \cdot 1000$  (dashed), where  $\phi = R_{ev}/R_e$  and  $\alpha_{eq}$  is the equilibrium fractionation coefficient. Both are expressed in ‰. The black, red and green lines are for ctrl, HighPrec and LowPrec respectively.

373 HighPrec and larger in LowPrec than in ctrl: rain evaporation has a weaker enriching  
 374 effect in HighPrec and a stronger enriching effect in LowPrec. This supports hypoth-  
 375 esis 3. In HighPrec near 4.5 km, near the melting level, there is even a small layer where  
 376  $\phi < 1$ : at this level, the rain evaporation has a depleting effect on the water vapor.

### 377 2.7 What controls the isotopic composition of rain evaporation?

378 Why is  $\phi$  smaller in HighPrec and higher in LowPrec than in ctrl? It could be be-  
 379 cause rain-vapor exchanges in a moister environment leads the evaporation to have a more  
 380 depleting effect (Lawrence et al., 2004; Risi et al., 2008), or because rain evaporation is  
 381 more depleted when the evaporated fraction is small (Risi et al., 2008; Tremoy et al., 2014),  
 382 or because the rain itself is more depleted. We aim here at quantifying these different  
 383 effects.

384 Figure 7a plots the vertical profiles of rain  $\delta D$  (solid). Below the melting level, the  
 385 rain is very close to isotopic equilibrium with the vapor (dashed). Above the melting level,  
 386 the rain is more enriched than if in equilibrium due to rain lofting. Near the melting level  
 387 for simulation HighPrec, the rain is anomalously depleted. This is due to snow melt. Since  
 388 the snow forms higher in altitude, it is more depleted than the rain. It thus imprints its  
 389 depleted signature on the rain when melting. In HighPrec, the moist middle troposphere  
 390 prevents most of the snow from sublimating: 24% of the precipitation is made of snow  
 391 at the melting level. The rain is thus strongly depleted by snow melt. In contrast, in ctrl  
 392 and LowPrec, the drier middle troposphere favors snow sublimation: only 8% and 3%  
 393 of the precipitation is made of snow at the melting level respectively.

394 The quick equilibration between the rain and vapor motivates us to use a simple  
 395 equation in which some mass  $q_{l0}$  of rain, with isotopic ratio  $R_{l0}$ , partially evaporates and  
 396 isotopically equilibrates with some mass  $q_{e0}$  of environment vapor, with isotopic ratio  
 397  $R_{e0}$ . As explained in text S2, if  $q_{l0} \gg q_{e0}$ , we get:

$$\phi = \frac{\lambda}{1 + (1 - f_{ev}) \cdot (\alpha_{eq} - 1)} \quad (2)$$

398 where  $\phi = R_{ev}/R_e$ ,  $\lambda = R_{i0}/R_{e0}$ ,  $R_{ev}$  is the isotopic ratio of the rain evapora-  
 399 tion flux,  $\alpha_{eq}$  is the equilibrium fractionation coefficient and  $f_{ev}$  is the fraction of the rain  
 400 that evaporates. Equation 2 tells us that the rain evaporation is more depleted as the  
 401 rain is more depleted relative to the vapor (quantified by  $\lambda$ ) and as the evaporated frac-  
 402 tion  $f_{ev}$  is smaller. This simple equation (Figure 7b, red) is able to approximate the sim-  
 403 ulated values of  $\phi$  (black) for the ctrl simulation and is able to capture the smaller and  
 404 larger values of  $\phi$  for HighPrec and LowPrec respectively (Figure 7c-d).

405 We find that below the melting level,  $\phi$  is smaller in HighPrec than in ctrl mainly  
 406 because  $f_{ev}$  is smaller (Figure 7c, green). Near the melting level,  $\phi$  is smaller in High-  
 407 Prec than in ctrl both because  $f_{ev}$  is smaller and because  $\lambda$  is smaller, i.e. the rain is more  
 408 depleted due to snow melt (Figure 7c, purple). In LowPrec, the effect of  $f_{ev}$  dominates  
 409 at most levels (Figure 7d).

## 410 2.8 Summary

411 To summarize, the previous sections suggest that rain evaporation in the lower tro-  
 412 posphere is a key ingredient of the vapor amount effect. The isotopic composition of the  
 413 rain evaporation flux mainly depends on the evaporated fraction of the rain, consistent  
 414 with Risi et al. (2008); Tremoy et al. (2014). Near the melting level in regimes of large-  
 415 scale ascent, it is also impacted by snow melt. We hypothesize that the isotopic effect  
 416 of rain evaporation propagates downward down to the SCL. To test this hypothesis and  
 417 to understand the underlying mechanisms, in the next section we develop a simple two-  
 418 column model.

## 419 3 A simple two-column model to quantify the relative contributions 420 of different processes

421 The previous section and previous studies provide a guide for developing our sim-  
 422 ple interpretative framework. First, the model needs to represent the effect of rain evap-  
 423 oration, highlighted as a key process in the previous section. Second, alternative hypothe-  
 424 ses for the “vapor amount effect” involve mixing between the subsident environment and  
 425 detrained water (Bailey et al., 2017) (hypothesis 4). This process also needs to be rep-  
 426 resented in our model. Third, the steepness of the  $q - \delta D_v$  relationship must be a key  
 427 ingredient, since it drives  $\delta D_v$  in the SCL and thus  $\delta D_v$  everywhere. Finally, the pre-  
 428 vious section has relied on the distinction between the environment and cloudy regions.  
 429 Keeping this distinction, we develop a two-column model.

### 430 3.1 Model equations and numerical application to LES outputs

#### 431 3.1.1 Balance equations

432 This model is inspired by the two-column model used to predict tropospheric rel-  
 433 ative humidity in Romps (2014) and  $\delta D_v$  profiles in Duan et al. (2018). The first col-  
 434 umn represents the cloudy regions, including cloudy updrafts and downdrafts, as a bulk  
 435 entraining plume. The second column represents the subsiding environment and precip-  
 436 itating downdrafts (Figure 8).

437 The mass balance for the air in the cloudy regions writes:

$$\frac{dM}{dz} = M \cdot (\epsilon - \delta) \quad (3)$$

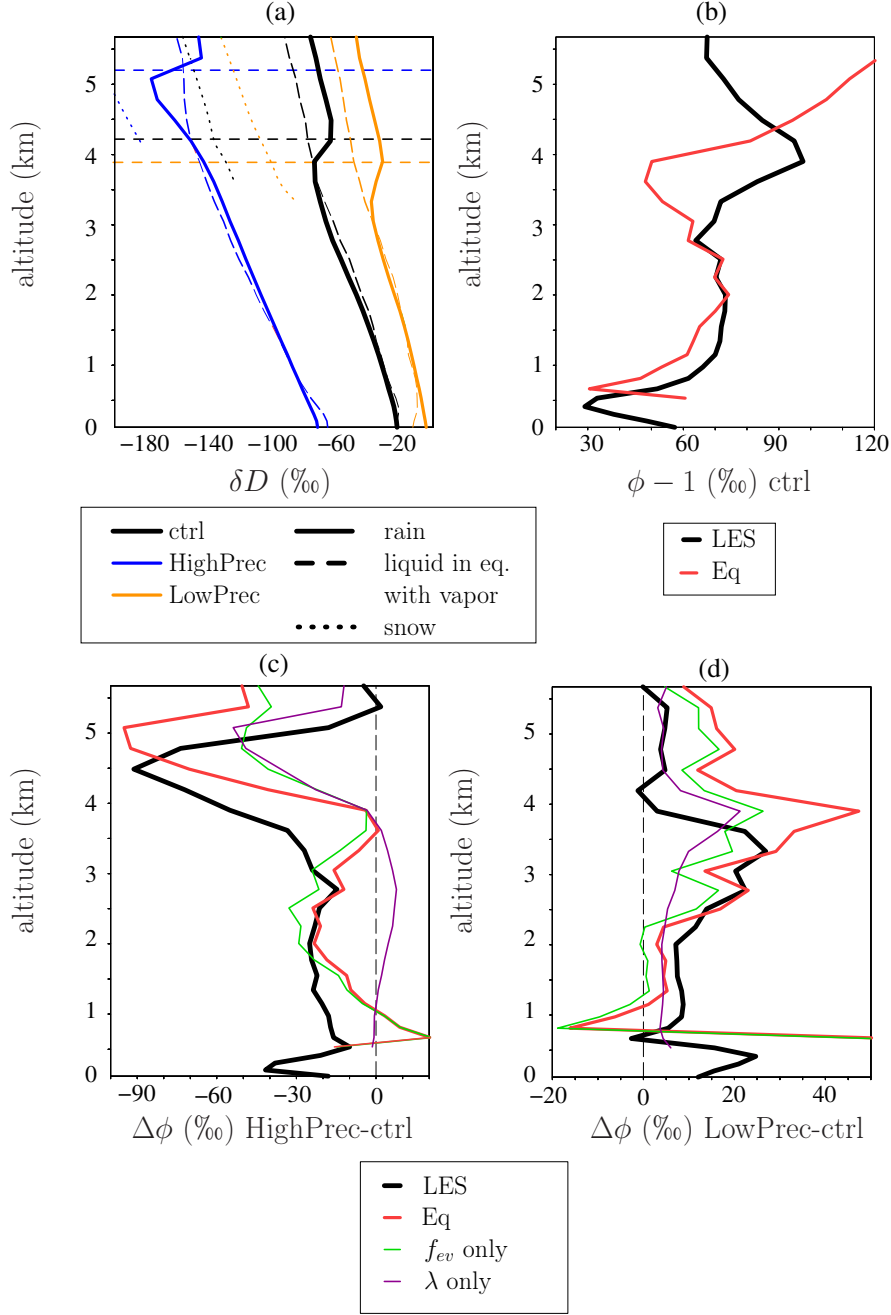


**Figure 7.** (a)  $\delta D$  profile for rain water (solid) and snow (dotted) falling in the environment. The liquid that would be in equilibrium with the vapor in the environment is shown in dashed. (b) Profile of  $\phi = R_{ev}/R_e$  simulated by the ctrl simulation (black, same as in Figure 6c black) and predicted by equation 2 (red). (c) Difference of  $\phi$  between HighPrec and ctrl simulated by the LES (black), predicted by the equation 2 (red), predicted by equation 2 if only  $f_{ev}$  varies (green) and if only  $\lambda$  varies (purple). (d) Same as (c) but for the difference between LowPrec and ctrl.

438 where  $M$  is the bulk mass flux in the cloudy regions (positive upward),  $\epsilon$  and  $\delta$  are  
439 the fractional entrainment and detrainment rates.

440 We assume that the  $q$  in the cloudy regions is at saturation, and call it  $q_s$ . The wa-  
441 ter balance in the cloudy regions writes:

$$\frac{d(Mq_s)}{dz} = \epsilon \cdot M \cdot q_e - \delta \cdot M \cdot q_s - c \quad (4)$$

442 where  $c$  is the condensation rate and  $q_e$  is the specific humidity in the environment.  
443 The terms on the right hand side represent the water input by entrainment of environ-  
444 ment air, the water loss by detrainment of cloudy air, and the water loss by condensa-  
445 tion respectively. We assume that all the condensed water is immediately lost by the cloudy  
446 regions to the environment, and evaporation of this lost water can occur in the sub-saturated  
447 environment only, as in Romps (2014).

448 We assume that mass is conserved within the domain, so that the flux in the en-  
449 vironment is  $-M$ . The large-scale ascent, when present, is taken into account through  
450 a humidity tendency, consistent with the LES set-up. We assume that the large-scale hu-  
451 midity tendency applies to the environment only, which is a first-order approximation  
452 justified by the small fraction of the domain that is covered by cloudy updrafts (less than  
453 10%). The water balance in the environment writes:

$$\frac{d(-Mq_e)}{dz} = -\epsilon \cdot M \cdot q_e + \delta \cdot M \cdot q_s + f_{ev} \cdot c - \eta \cdot M \cdot \frac{\partial q_e}{\partial z} \quad (5)$$

454 where  $f_{ev}$  is the fraction of the cloud or precipitating water that evaporates in the  
455 environment,  $\eta = M_{LS}/M$  and  $M_{LS}$  is the domain-mean large-scale mass flux. The terms  
456 on the right hand side represents the water loss by entrainment into cloudy regions, wa-  
457 ter input by the detrainment of cloudy air, partial evaporation of condensed water and  
458 water input by large-scale vertical advection.

459 Regarding water isotopes, we assume that the cloud water removed by condensa-  
460 tion is in isotopic equilibrium with the cloudy region water vapor. The isotopic balance  
461 in the cloudy regions thus writes:

$$\frac{d(Mq_s \cdot R_s)}{dz} = \epsilon \cdot M \cdot q_e \cdot R_e - \delta \cdot M \cdot q_s \cdot R_s - c \cdot \alpha_{eq} \cdot R_s \quad (6)$$

462 where  $\alpha_{eq}$  is the equilibrium fractionation coefficient,  $R_s$  is the isotopic ratio in the  
463 cloudy regions and  $R_e$  is the isotopic ratio in the environment.

464 The isotopic balance in the environment writes:

$$\frac{d(-Mq_e \cdot R_e)}{dz} = -\epsilon \cdot M \cdot q_e \cdot R_e + \delta \cdot M \cdot q_s \cdot R_s + f_{ev} \cdot c \cdot \phi \cdot R_e - \eta \cdot M \cdot \frac{\partial (q_e R_e)}{\partial z} \quad (7)$$

465 where  $\phi = R_{ev}/R_e$  and  $R_{ev}$  is the ratio of the precipitation evaporation flux.

### 466 **3.1.2 Other simplifying assumptions and differential equations**

467 To simplify the equations, as in Romps (2014) we assume that  $q_s$  is an exponen-  
468 tial function of altitude:

$$q_s = q_s(z_0) \cdot e^{-\gamma \cdot (z-z_0)} \quad (8)$$

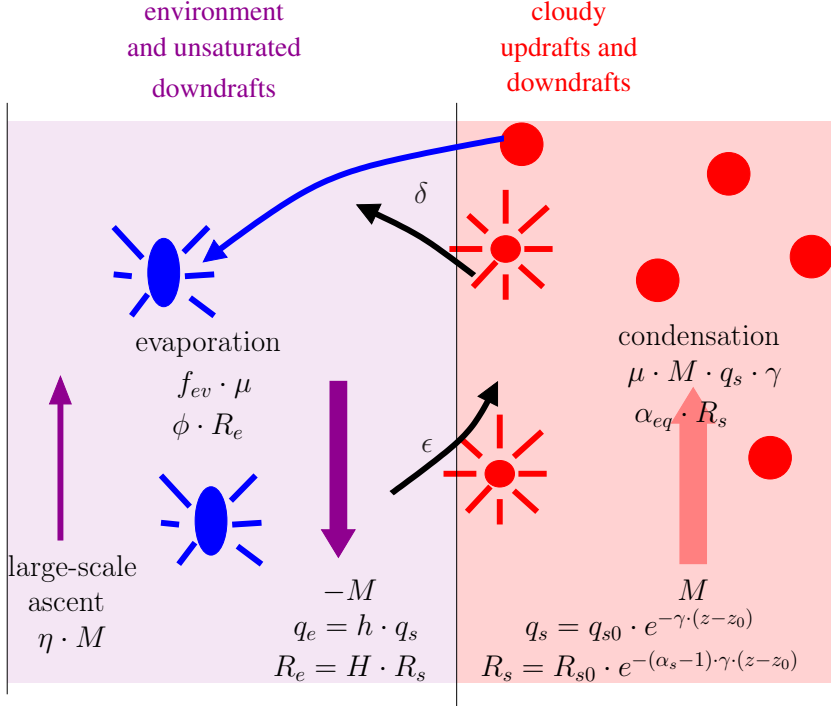


**Figure 8.** Schematic view of the simple two-column model, and definition of the main variables.

469 where  $\gamma$  is a lapse rate in  $m^{-1}$  calculated as  $d \ln(q_s)/dz$ .

470 For isotopes, we assume that the  $R_s$  is a power function of  $q_s$ , consistent with a  
471 Rayleigh distillation:

$$R_s = R_s(z_0) (q_s/q_{s0})^{\alpha_s - 1}$$

472 Coefficient  $\alpha_s$  represents the steepness of the  $q - \delta D_v$  gradient in cloudy regions  
473 and remains to be estimated. As in Duan et al. (2018),  $R_s$  is thus an exponential func-  
474 tion of altitude:

$$R_s = R_s(z_0) \cdot e^{-(\alpha_s - 1) \cdot \gamma \cdot (z - z_0)} \quad (9)$$

475 We set:

$$q_e = h \cdot q_s$$

$$R_e = H \cdot R_s$$

476 Combining equation 5 with equations 3 and 8, we get the following differential equa-  
477 tion for  $h$ :

$$\frac{\partial h}{\partial z} = h \cdot \gamma - \frac{\delta}{1 - \eta} (1 - h) - \frac{f_{ev} \cdot \mu \cdot \gamma}{1 - \eta} \quad (10)$$

478 where  $\mu = c/(M \cdot q_s \cdot \gamma)$  represents the ratio of actual condensation ( $c$ ) relative  
 479 to the condensation if the ascent was adiabatic ( $M \cdot q_s \cdot \gamma$ ). Similarly, combining equa-  
 480 tions 7 with equations 5 and 9, we get the following differential equation for  $H$ :

$$\frac{\partial H}{\partial z} = H \cdot \gamma \cdot (\alpha_s - 1) - \frac{\delta}{h \cdot (1 - \eta)} \cdot (1 - H) - \frac{f_{ev} \cdot \mu \cdot \gamma}{h \cdot (1 - \eta)} \cdot H \cdot (\phi - 1) \quad (11)$$

481 Note that these equations are only valid as long as  $\eta < 1$ , which will be the case  
 482 in all our simulations (section 3.1.4). We now have two equations with four unknowns:  
 483  $h$ ,  $H$ ,  $\mu$  and  $\alpha_s$ . The condensation efficiency  $\mu$  can be deduced from equations 4:

$$\mu = 1 - \frac{\epsilon}{\gamma} \cdot (1 - h) \quad (12)$$

484 This equation, similar to one in Romps (2014), reflects the fact that condensation  
 485 efficiency decreases when entrainment  $\epsilon$  increases and when the entrained air is drier. If  
 486  $\epsilon = 0$  or  $h = 1$ , then  $\mu = 1$ .

487 Similarly, the  $q - \delta D_v$  steepness  $\alpha_s$  in cloudy air can be deduced from equation  
 488 6:

$$\alpha_s - 1 = \mu \cdot (\alpha_{eq} - 1) + \frac{\epsilon}{\gamma} \cdot h \cdot (1 - H) \quad (13)$$

489 This equation tells us that two effects control the steepness of the  $q - \delta D_v$  gra-  
 490 dient. First, there is a ‘‘dilution effect’’: if dry air is entrained, then the condensation  
 491 efficiency  $\mu$  decreases. This reduces  $\alpha_s$  compared to  $\alpha_{eq}$ , i.e. compared to what we would  
 492 expect from Rayleigh distillation. Second, there is an ‘‘isotopic contrast effect’’: if de-  
 493pleted water vapor is entrained ( $H < 1$ ), then  $\alpha_s$  becomes steeper. This is how a de-  
 494pleting effect of rain evaporation in the environment can translate into a larger steep-  
 495ness in both regions, and eventually more depleted SCL.

### 496 3.1.3 Numerical solutions

497 To get analytical solutions for  $h$  and  $H$ , Romps (2014) and Duan et al. (2018) as-  
 498sume that  $h \cdot \frac{\partial q_s}{\partial z} \gg q_s \cdot \frac{\partial h}{\partial z}$  and that  $H \cdot \frac{\partial R_s}{\partial z} \gg R_s \cdot \frac{\partial H}{\partial z}$ . This allows them to calculate  $h$   
 499 and  $H$  as the solutions of a simple linear equation and of a second order polynomial re-  
 500spectively. However, there are two issues with these solutions. First, although these so-  
 501lutions behave reasonably for  $h$  (Romps, 2014), they become very noisy, unstable or un-  
 502realistic for  $H$  when values for  $\epsilon$ ,  $\delta$  and  $f_{ev}$  that are diagnosed from LES outputs. This  
 503is because a powerful positive feedback exists between  $\alpha_s$  and  $H$ : as  $H$  decreases, more  
 504depleted vapor is entrained in updrafts which increases the steepness  $\alpha_s$ ; in turn, the stronger  
 505steepness  $\alpha_s$  makes the subsidence more efficient at depleting the environment, further  
 506decreasing  $H$ . Duan et al. (2018) circumvented this problem by assuming  $\epsilon$  and  $\delta$  that  
 507are constant with altitude and equal to each other, but it is at the cost of artificially re-  
 508ducing freedom for the solutions. Second, our hypothesis is that rain evaporation near  
 509the melting level affects the isotopic profiles down to the SCL. We thus want each alti-  
 510tude to feel the memory of processes at higher altitudes. The term with  $\frac{\partial H}{\partial z}$  is thus a  
 511key ingredient in our framework.

512 Therefore, we choose to numerically solve the differential equations 10 and 11. We  
 513start from an altitude of 5 km with  $h = 0.8$  and  $H - 1 = -10\%$ . We do not start  
 514above 5 km because entrainment is more difficult to diagnose above the melting level (sec-  
 515tion 3.1.4). We integrate equations 10 and 11 down to the SCL top around 500 m. The  
 516resulting  $h$  profile is a function of the profiles of 5 input parameters:  $\gamma$ ,  $\epsilon$ ,  $\delta$ ,  $f_{ev}$  and  $\eta$

517 . The  $H$  profile is a function of 7 input parameters:  $\gamma$ ,  $\epsilon$ ,  $\delta$ ,  $f_{ev}$ ,  $\eta$ ,  $\alpha_{eq}$  and  $\phi$ . These in-  
 518 put parameters are all diagnosed from the LES simulations as detailed below. In each  
 519 LES level, the input parameters are assumed constant and equations 10 and 11 are in-  
 520 tegrated within each layer over 50 sub-layers.

### 521 3.1.4 Diagnosed input parameters

522 Parameters  $f_{ev}$ ,  $\alpha_{eq}$  and  $\phi$  were already plotted in Figure 6 and discussed in sec-  
 523 tion 2.6. Parameter  $\gamma$  is calculated from domain-mean profiles. It is steeper in ctrl than  
 524 in  $\omega-60$  because of the steeper temperature gradient resulting from the drier air (Fig-  
 525 ure 9a). Parameter  $\eta = M_{LS}/M$  is calculated from the net upward mass flux in cloudy  
 526 regions  $M$  (Figure 9b), which is calculated as the average vertical velocity in cloudy re-  
 527 gions multiplied by the area fraction of the cloudy region. Entrainment  $\epsilon$  is diagnosed  
 528 by using the conservation of the frozen moist static energy  $m$  (e.g. Hohenegger and Brether-  
 529 ton (2011); Del Genio and Wu (2010)):

$$\frac{\partial m_s}{dz} = \epsilon \cdot (m_e - m_s)$$

530 where  $m_s$  and  $m_e$  are the frozen moist static energy in the cloudy region and the  
 531 environment respectively. The application of this equation is limited to the lower tro-  
 532 posphere. Above the melting level, we would need to account for the precipitation of ice  
 533 (Pauluis & Mrowiec, 2013) and for the lofting of rain. Therefore, we arbitrarily set a min-  
 534 imum of  $\epsilon = 0.5 \text{ km}^{-1}$  above the melting level. Entrainment is maximal in the sub-cloud  
 535 layer, and decreases exponentially with height (Figure 9c), consistent with previous stud-  
 536 ies (Del Genio & Wu, 2010; De Rooy et al., 2013).

537 Finally, detrainment  $\delta$  is deduced from  $\epsilon$  and  $M$  using equation 3. Detrainment shows  
 538 the typical trimodal distribution (Johnson et al., 1999) (Figure 9d), with a first max-  
 539 imum just above the SCL top corresponding to the detrainment of shallow convection,  
 540 a second maximum near the melting level corresponding to the detrainment of conges-  
 541 tus convection, and a third maximum in the upper troposphere corresponding to the deep  
 542 convection (not shown in Figure 9d).

### 543 3.1.5 Closure in the sub-cloud layer

544 To calculate the full  $\delta D$  profiles, we need as initial condition the isotopic ratio in  
 545 the SCL. With this aim, we use a simple version of the SCL model of Risi et al. (2020).  
 546 We assume that water enters the SCL through surface evaporation and through down-  
 547 drafts at the SCL top, and exits the SCL through updrafts at the SCL top. We neglect  
 548 large-scale forcing and rain evaporation, since they have a small impact in the SCL (Risi  
 549 et al., 2020). The air flux of updrafts equals that of downdrafts. We define  $r_u = q_u/q_1$   
 550 and  $r_d = q_d/q_1$ , where  $q_1$  is the mixing ratio in the SCL and  $q_u$  and  $q_d$  are the mixing  
 551 ratios in updrafts and downdrafts at the SCL top. We assume that the water vapor is  
 552 more enriched as the air is moister, following a logarithmic function:  $R_u = R_1 \cdot r_u^{\alpha_u - 1}$   
 553 and  $R_d = R_1 \cdot r_d^{\alpha_d - 1}$  where  $R_u$  and  $R_d$  are isotopic ratios in updrafts and downdrafts,  
 554 and  $\alpha_u$  and  $\alpha_d$  are the  $q-\delta D_v$  steepness coefficients for updrafts and downdrafts. Wa-  
 555 ter and isotopic budgets yield:

$$R_1 = \frac{R_{oce}/\alpha_{eq}(SST)}{h_1 + \alpha_K \cdot (1 - h_1) \cdot \frac{r_u^{\alpha_u} - r_d^{\alpha_d}}{r_u - r_d}} \quad (14)$$

556 where  $R_{oce}$  is the isotopic ratio at the ocean surface,  $\alpha_{eq}(SST)$  is the equilibrium  
 557 fractionation coefficient at the sea surface temperature,  $\alpha_K$  is kinetic fractionation co-  
 558 efficient (Merlivat & Jouzel, 1979) and  $h_1$  is the relative humidity normalized at the SST

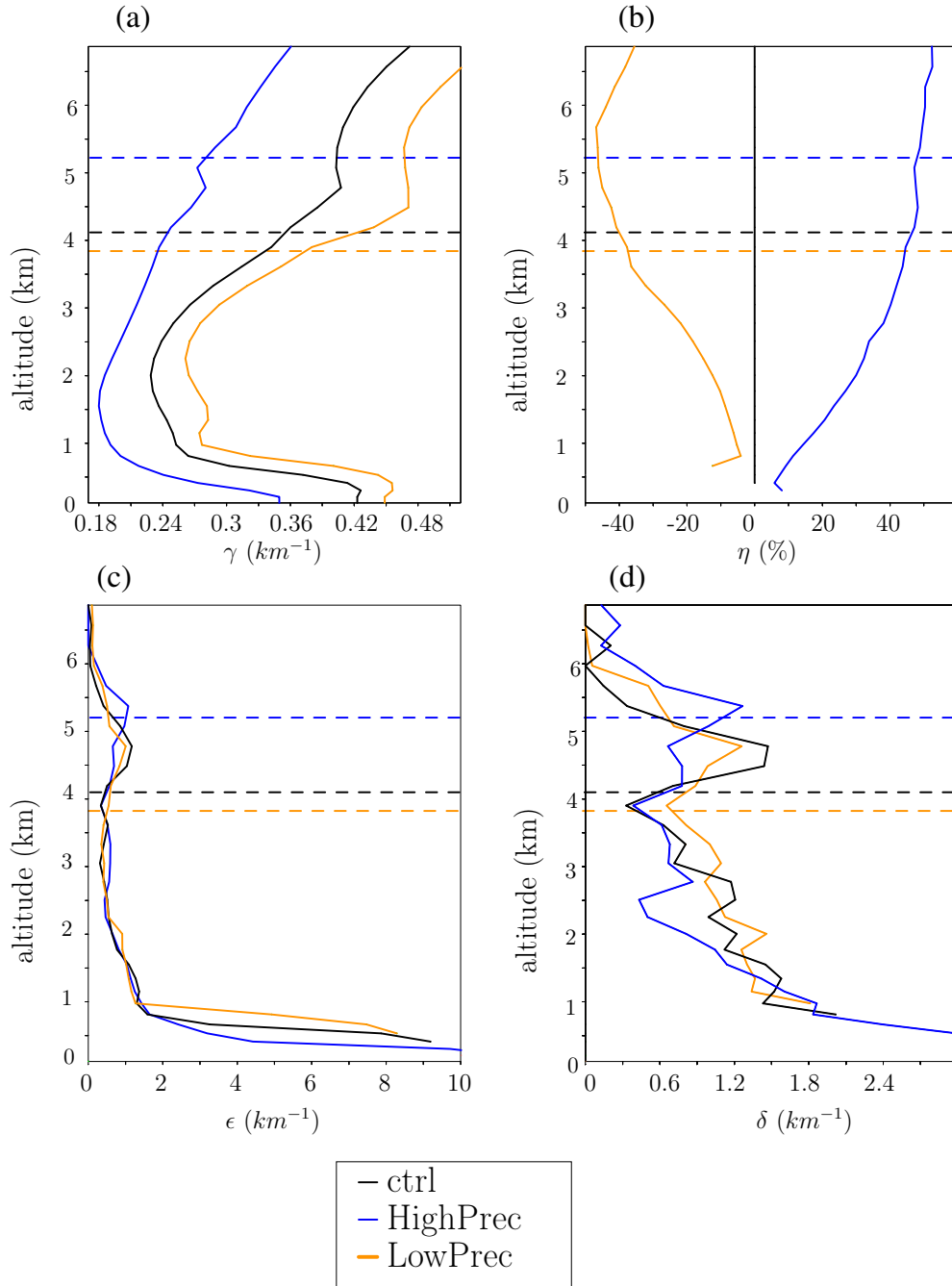


**Figure 9.** Input parameters for the simple model, for ctrl (black), HighPrec (blue) and LowPrec (orange). (a) saturation specific humidity lapse rate  $\gamma$ ; (b) ratio of large-scale vertical mass flux over the cloudy mass flux; (c) entrainment rate; (d) detrainment rate.

559 and accounting for ocean salinity:  $h_1 = q_1/q_{sat}^{surf}(SST)$ ,  $q_{sat}^{surf}(SST) = 0.98 \cdot q_{sat}(SST)$   
 560 and  $q_{sat}$  is the humidity saturation as a function of temperature at the sea level pres-  
 561 sure. We assume  $\delta D_{oce} = 0\%$  and  $h_1$  is diagnosed from the LES.

562 For  $r_u$  and  $r_d$ , we use values for the ctrl simulation, because small changes in  $r_u$   
 563 and  $r_d$  across simulations have only a marginal impact on  $R_1$  (Risi et al., 2020). Follow-  
 564 ing Risi et al. (2020), we set  $r_u - 1 = 1.44\%$  and  $r_d - 1 = -0.38\%$ . For  $\alpha_u$  and  $\alpha_d$ , Risi et  
 565 al. (2020) had shown that they scale with  $\alpha_z$  values just above the SCL top, but with  
 566 larger values especially for simulations with large-scale ascent. We use an empirically-  
 567 fitting function:  $\alpha_u = \alpha_d = 1 + 100 \cdot (\widetilde{\alpha}_z - 1)^3$ , where  $\widetilde{\alpha}_z = 1 + \frac{\ln(R(z_{SCT})/R(z_{SCT}+1\text{ km}))}{\ln(q(z_{SCT})/d(z_{SCT}+1\text{ km}))}$   
 568 and  $z_{SCT}$  is the altitude of SCL top.

569 Finally, since the updraft region covers only a very small fraction of the domain,  
 570 we assume that  $R_e(z_{SCT}) \simeq R_1$ .

571 The procedure to calculate the full  $\delta D_v$  profiles is as follows:

- 572 1. vertical profiles for  $h$ ,  $H$  and  $\alpha_s$  are calculated through a downward integration  
 573 of equations 10-13 following section 3.1.3.
- 574 2. The vertical profile for a normalized version of  $R_s$ ,  $R_{s,norm}$  that satisfies  $R_{s,norm}(z_{SCT}) =$   
 575 1, is calculated based on the  $\alpha_s$  profile through an upward integration.
- 576 3. The vertical profile for a normalized version of  $R_e$ ,  $R_{e,norm}$ , is calculated as  $R_{e,norm} =$   
 577  $R_{s,norm} \cdot H$ .
- 578 4. From the  $R_{e,norm}$  profile,  $\widetilde{\alpha}_z$  is estimated.
- 579 5. From  $h_1$  and  $\widetilde{\alpha}_z$ ,  $R_1$  is estimated.
- 580 6. The full  $R_e$  profile can finally be calculated so that  $R_e(z_{SCT}) \simeq R_1$ :  $R_e = R_{e,norm} \cdot$   
 581  $R_1/H(z_{SCT})$ .

### 582 **3.1.6 Evaluation of the two-column model**

583 The two-column model successfully captures the order of magnitude and the shape  
 584 of the vertical profile of  $h$  for the ctrl simulation (Figure 10a), as well as the moister tropo-  
 585 sphere in HighPrec and the drier troposphere in LowPrec (Figure 10b-c).

586 It successfully captures the vertical profile of  $\delta D_v$  (Figure 10b) and the more de-  
 587 pleted troposphere in HighPrec but underestimate the  $\delta D_v$  difference by about half (Fig-  
 588 ure 10e). It also captures the more enriched troposphere in LowPrec but again under-  
 589 estimate the  $\delta D_v$  difference especially in the middle troposphere (Figure 10f). Similarly,  
 590 it approximately captures the steepness  $\alpha_z$  and the sign of the  $\alpha_z$  differences across sim-  
 591 ulations, but underestimates the  $\alpha_z$  differences (Figure 10g-i).

592 These mismatches are caused by mismatches in the estimate of the relative enrich-  
 593 ment of the environment relative to the cloudy region  $H$ . Although it is reasonably well  
 594 predicted for the ctrl simulation (Figure 10j), the model fails to simulate the smaller  $H$   
 595 for HighPrec in the middle troposphere and the larger  $H$  for LowPrec almost everywhere.  
 596 The two-column model overestimates the impact of  $\eta$  and predicts a behavior for  $H$  that  
 597 is too similar to that of  $h$ . We could not find the exact reason for this shortcoming, but  
 598 we have to acknowledge that the two-column model hides many horizontal heterogeneities.  
 599 We will have to keep this shortcoming in mind when interpreting the results.

### 600 **3.2 Decomposition of relative humidity and $\delta D_v$ variations**

601 To estimate the impact of the different input parameters on the  $h$  and  $\delta D_v$  pro-  
 602 files, we modify them one by one from the ctrl simulation to the HighPrec and from the  
 603 ctrl simulation to LowPrec simulations.

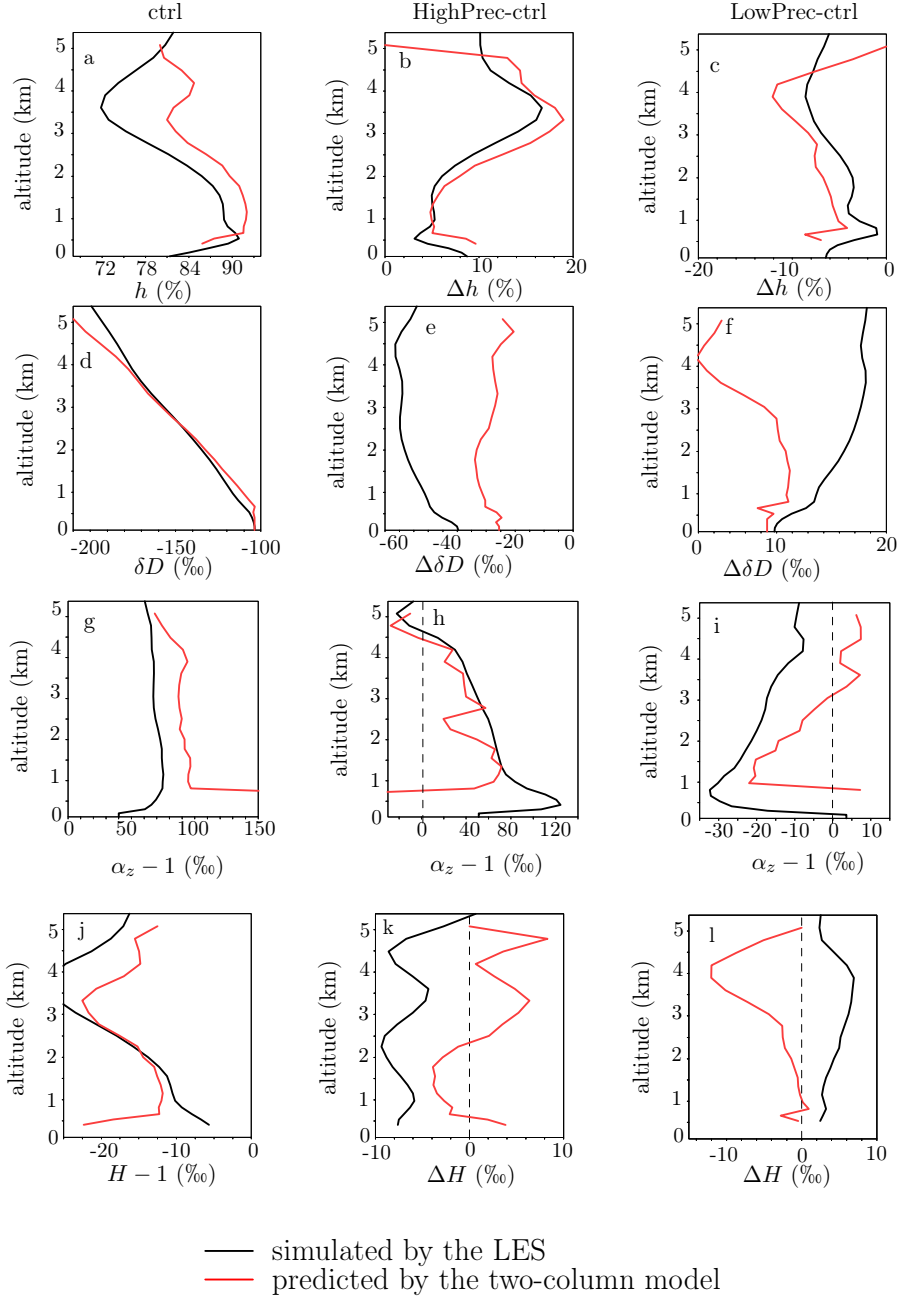


**Figure 10.** (a) Relative humidity  $h$  simulated by the LES (black) and predicted by the two-column model (red) for the ctrl simulation. (b) Same as (a) but for the difference between HighPrec and ctrl. (c) Same as (b) but for the difference between LowPrec and ctrl. (d-f) Same as (a-c) but for the water vapor  $\delta D$ . (g-i) Same as (a-c) but for the steepness  $\alpha_z$ . (j-l) Same as (a-c) but for the relative enrichment of the environment relative to the updrafts  $H$ .

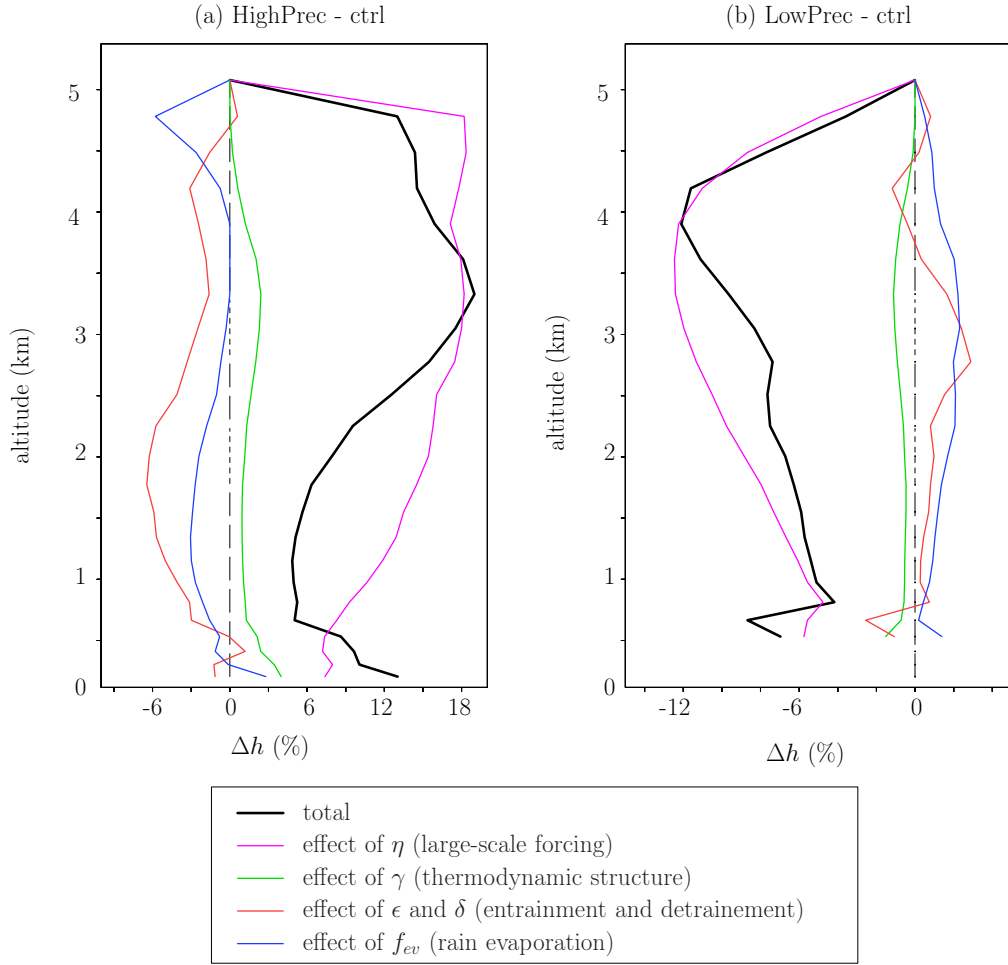


**Figure 11.** (a) Relative humidity difference between HighPrec and ctrl predicted by the two-column model (black) and its contributions from variations of input parameters one by one:  $\eta$  (pink),  $\gamma$  (green),  $\epsilon$  and  $\delta$  (red) and  $f_{ev}$  (blue). (b) Same as (a) but for the difference between LowPrec and ctrl.

604

### 3.2.1 Decomposition of relative humidity

605

606

607

608

609

The moister troposphere in HighPrec is mainly due to the larger  $\eta$ , i.e. the direct moistening effect of large-scale ascent (Figure 11a). The thermodynamic structure, entrainment, detrainment and rain evaporation have a much smaller effect. Similarly, The drier troposphere in LowPrec is mainly due to the more negative  $\eta$ , i.e. the direct drying effect of large-scale descent (Figure 11b).

610

611

612

Note that the direct effect of  $\eta$  on  $h$  in the environment may be overestimated in our simulations by prescribing a large-scale vertical velocity profile that is horizontally constant (Bao et al., 2017).

613

### 3.2.2 Dilution effect on $\delta D_v$

614

615

616

A first effect impacting  $\delta D_v$  profiles is the dilution by entrainment (section 3.1.2). In the absence of entrainment ( $\epsilon = 0$ ), the steepness in the updraft column would be  $\alpha_s = \alpha_{eq}$  (Figure 12a, black). Because dry air is entrained, the condensation rate is re-

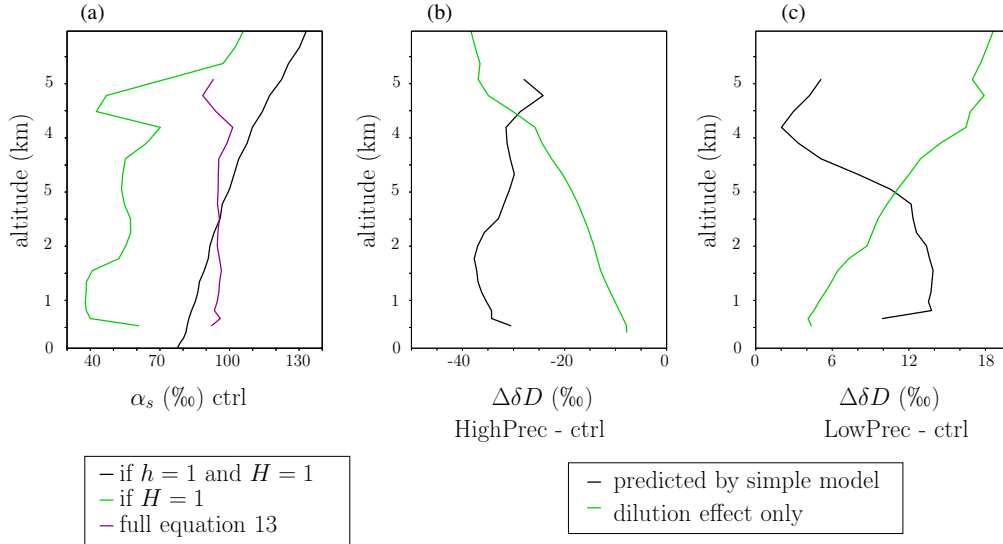


**Figure 12.** (a) Fractionation coefficient  $\alpha_{eq}$  (black), corresponding to the steepness in the cloudy column  $\alpha_s$  if  $h = 1$  and  $H = 1$ ; steepness  $\alpha_s$  predicted if  $h < 1$  and  $H = 1$  ( $\alpha_s = 1 + \mu \cdot (\alpha_{eq} - 1)$ ) (green); steepness  $\alpha_s$  from the full equation 13 (purple). (b) Difference in  $\delta D_v$  from ctrl to HighPrec predicted by the two-column model (black) and predicted if accounting only for the dilution effect (green). (c) Same as (b) but for LowPrec.

617 deduced by the factor  $\mu$  following equation 12. According to equation 13, this reduces the  
 618 steepness (Figure 12a, green). This effect of entrainment can be understood as a mixing  
 619 process: as the air rises and condensation proceeds, the remaining air is mixed with  
 620 dry air from entrainment and with droplets that evaporate. Consistent with the concave-  
 621 down shape of the mixing lines, this leads to a reduction of the  $q$ - $\delta D_v$  steepness (Fig-  
 622 ure 1, orange and cyan).

623 As a consequence of this “dilution effect”, tropospheric  $\delta D_v$  is less depleted than  
 624 predicted by Rayleigh distillation. Since the troposphere is moister in HighPrec, entrained  
 625 air leads to less evaporation of cloud droplets than in ctrl. This weaker “dilution effect”  
 626 contributes to more depleted  $\delta D_v$  in HighPrec (Figure 12b, green). Reciprocally, since  
 627 the troposphere is drier in LowPrec, the stronger “dilution effect” contributes to the more  
 628 enriched  $\delta D_v$  in LowPrec (Figure 12c, green). Quantitatively, the contribution of this  
 629 dilution effect on the SCL  $\delta D_v$  difference is 29% for HighPrec and 47% for LowPrec (ta-  
 630 ble 2). The contribution increases with altitude.

631 Note that the two-column model likely overestimates this contribution, because of  
 632 the shortcomings mentioned in section 3.1.6. The fact that only one third of the  $\delta D_v$  dif-  
 633 ference remains when post-condensation effects are turned off (section 2.4) confirms that  
 634 these contributions are overestimated.

### 635 3.2.3 Decomposition of $\delta D_v$

636 In HighPrec, the more depleted troposphere is driven primarily by the effect of the  
 637 smaller  $\phi$ , i.e. the more depleted rain evaporation (Figure 13a, cyan). It explains 147%  
 638 of the  $\delta D_v$  difference in the SCL (Table 2). The smaller rain evaporated fraction (smaller  
 639  $f_{ev}$ ) is the second main contributor (Figure 13a, blue, 43% in the SCL). This positive  
 640 contribution is explained by the fact that evaporation has an overall enriching effect. The  
 641 third main contributor is the larger  $\eta$  (i.e. large-scale ascent), contributing to 26% of the

**Table 1.** Difference of  $\delta D_v$  in the SCL between HighPrec and ctrl and between LowPrec and ctrl simulated by the LES and predicted by the two-column model, and the contribution of the dilution effect.

Difference in SCL $\delta D_v$ from ctrl	HighPrec	LowPrec
Total simulated by the LES (%)	-40	10
Total predicted by the two-column model (%)	-30	11
Dilution effect (% <sub>0</sub> , %)	-9 (29%)	5 (47%)

642  $\delta D_v$  difference. This contribution corresponds mainly to the “dilution effect” explained  
 643 in section 3.2.2. The sum of these contributions exceeds 100%, because there are some  
 644 dampening effects, especially  $h_1$ : the moister surface relative humidity reduces the ki-  
 645 netic fractionation during surface evaporation.

646 In LowPrec,  $\eta$  becomes the main contribution to the  $\delta D_v$  difference in the SCL (126%),  
 647 through the dilution effect (Figure 13b, pink, Table 2). The effect of the larger  $\phi$ , i.e. the  
 648 more enriched rain evaporation, contributes to 36% to the  $\delta D_v$  difference in the SCL.

649 This decomposition can be reconciled with the result that about one third of the  
 650  $\delta D_v$  difference from ctrl to HighPrec remains when the fractionation during condensate  
 651 evaporation is de-activated. This remaining difference is associated with (1) the dilution  
 652 effect, and (2) the portion of the  $\phi$  contribution that is due to the more depleted rain  
 653 due to more snow melt. The fact that the sum of this two contributions exceeds one third  
 654 suggests that the underestimate of  $\delta D_v$  variations by the simple model is due to under-  
 655 estimating the effect of rain evaporation.

656 We note that the relative contributions of the different processes are very homo-  
 657 geneous in the vertical. For example, in the SCL, half of the contribution of  $\phi$  comes from  
 658  $\phi$  above 3 km. This shows the strong “memory” of water vapor  $\delta D$ , which integrates pro-  
 659 cesses downwards in the environment column, and then upward in the cloudy column.

## 660 4 Conclusion

### 661 4.1 Summary

662 The amount effect, i.e. the observed decrease in precipitation  $\delta D$  as precipitation  
 663 rate increases, is the most salient feature in monthly-mean isotopic observations over trop-  
 664 ical oceans (Dansgaard, 1964). We confirm here that it is intimately related to the “va-  
 665 por amount effect”, i.e. the observed decrease in water vapor  $\delta D$  as precipitation rate  
 666 increases (Worden et al., 2007). This study gives a comprehensive and quantitative un-  
 667 derstanding of the processes underlying the vapor amount effect, at least in our LES sim-  
 668 ulations. This understanding is illustrated in Figure 14:

- 669 1. When the troposphere is moister (in terms of relative humidity), less snow sub-  
 670 limates and thus more snow is available for melting. Snow melt results in rain that  
 671 is more depleted relative to a liquid in equilibrium with the vapor, which leads to  
 672 more depleted rain evaporation flux. When the troposphere is moister, the rain  
 673 evaporated fraction is also smaller, making the rain evaporation flux even more  
 674 depleted.
- 675 2. The more depleted evaporation depletes the environment more efficiently relative  
 676 to clouds. When this more depleted environment is entrained into the clouds, it

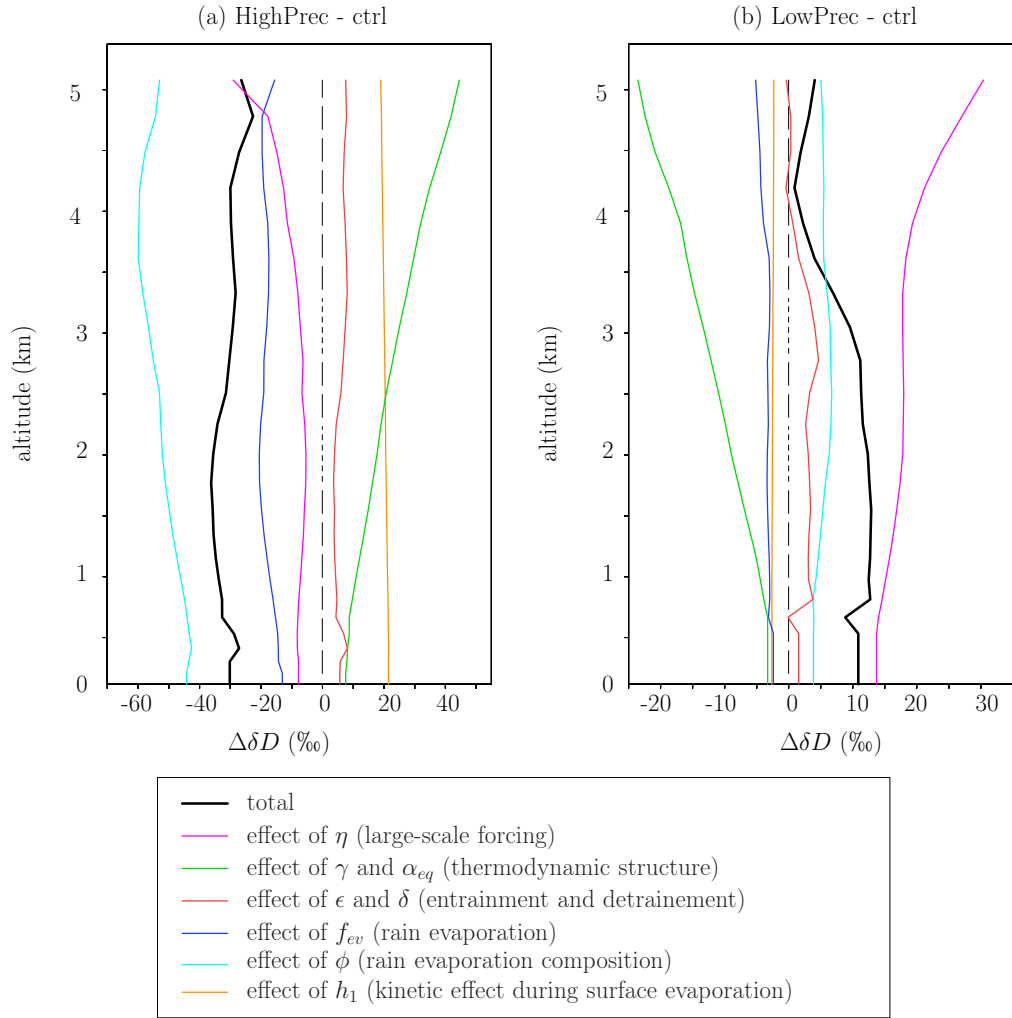


**Figure 13.** (a)  $\delta D_v$  difference between HighPrec and ctrl predicted by the two-column model (black) and its contributions from variations of input parameters one by one:  $\eta$  (pink),  $\gamma$  and  $\alpha_{eq}$  (green),  $\epsilon$  and  $\delta$  (red),  $f_{ev}$  (blue),  $\phi$  (cyan) and  $h_1$  (orange). (b) Same as (a) but for the difference between LowPrec and ctrl.

**Table 2.** Difference of  $\delta D_v$  in the SCL between HighPrec and ctrl and between LowPrec and ctrl simulated by the LES and predicted by the two-column model, and the contribution of different effects. The sum of all the different effects, except the line “Including  $\phi$  above 3 km”, is 100% of the predicted  $\delta D_v$  difference. The line “Including  $\phi$  above 3 km” is a part of “Effect of  $\phi$ ”

SCL $\delta D_v$ difference from ctrl	HighPrec	LowPrec
Total simulated by the LES (%)	-40	10
Total predicted by the two-column model (%)	-30	11
Effect of $\gamma$ and $\alpha_{eq}$ (% <sub>00</sub> , %)	8 (-25%)	-3 (-30%)
Effect of $\epsilon$ and $\delta$ (% <sub>00</sub> , %)	6 (-19%)	2 (14%)
Effect of $\eta$ (% <sub>00</sub> , %)	-8 (26%)	14 (126%)
Effect of $f_{ev}$ (% <sub>00</sub> , %)	-13 (43%)	-2 (-22%)
Effect of $\phi$ (% <sub>00</sub> , %)	-44 (147%)	4 (36%)
Including $\phi$ above 3 km (% <sub>00</sub> , %)	-23 (76%)	2 (23%)
Effect of $h_1$ (% <sub>00</sub> , %)	22 (-72%)	-3 (-24%)

- 677 makes the  $q-\delta D_v$  vertical gradient steeper. In turn, the steeper  $q-\delta D_v$  gradi-  
678 ent makes the subsidence more efficient at depleting the environment, in a posi-  
679 tive feedback that makes the  $q-\delta D_v$  gradient even steeper. Overall, this mech-  
680 anism allows to propagate the isotopic anomalies associated with rain evapora-  
681 tion downwards.
- 682 3. When the troposphere is moister, the dilution of cloudy air by entrainment is weaker.  
683 Water vapor condenses more efficiently, which also contributes to the steeper  $q-$   
684  $\delta D_v$  vertical gradient.
  - 685 4. The steeper  $q-\delta D_v$  gradient in the lower troposphere makes updrafts and down-  
686 drafts at the SCL top more efficient in depleting the SCL water vapor (Risi et al.,  
687 2020).
  - 688 5. Finally, since the more depleted SCL vapor serves as the initial condition for the  
689 full  $\delta D_v$  vertical profiles, the water vapor is more depleted at all altitudes in the  
690 troposphere.

691 Coming back to our initial hypotheses to explain the vapor amount effect, the dom-  
692 inant role of rain evaporation and rain-vapor diffusive exchanges confirms hypothesis 3  
693 (Lawrence et al., 2004; Risi et al., 2008; Lee & Fung, 2008). The role of entrainment in  
694 diluting cloudy air and reducing their condensation efficiency is reminiscent of hyptho-  
695 thesis 4.

696 We notice that the root of the vapor amount effect in the water vapor is higher rel-  
697 ative humidity, with a triple effect on reducing (1) the sublimation of snow aloft, (2) the  
698 fraction of rain that evaporates, and (3) the dilution of cloudy air by entrainment. This  
699 explains why the amount effect can be observed only when the precipitation increase is  
700 associated with a change in the large-scale circulation (Bony et al., 2008; Moore et al.,  
701 2014; Bailey et al., 2017; Risi et al., 2020). While the tropospheric relative humidity is  
702 very sensitive to the large-scale circulation, it is almost invariant with sea surface tem-  
703 perature (Romps, 2014). For example, if precipitation increases because sea surface tem-  
704 perature increases without any change in large-scale circulation, then the tropospheric

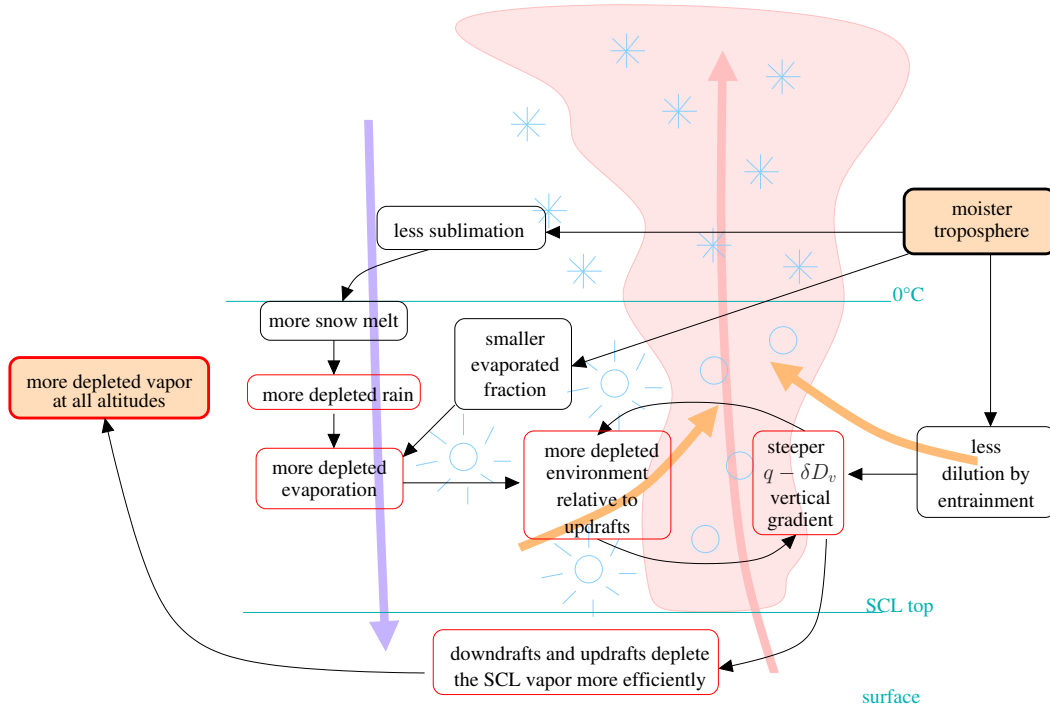


**Figure 14.** Schematic summarizing how a moister troposphere leads to more depleted vapor in the troposphere. The black and red boxes represent standard water processes and isotopic processes respectively.

705 humidity would remain almost constant (Romps, 2014), so the above-mentioned mech-  
 706 anism cannot take place and there is no amount effect.

## 707 4.2 Discussion and perspectives

708 This study has investigated processes controlling isotopic profiles in idealized con-  
 709 ditions. In particular, large-scale horizontal gradients in humidity and  $\delta D_v$  were neglected.  
 710 In reality, these gradients are expected to dampen the humidity and  $\delta D$  variations as  
 711 a function of large-scale vertical velocity (Risi et al., 2019).

712 To assess to what extent our idealized simulations in radiative-convective equi-  
 713 librium over the ocean are relevant for interpreting observations, it would be useful to  
 714 compare our LES simulations with different large-scale velocities to in-situ and remote-  
 715 sensing observations. This raises the question of the spatial scales at which the amount  
 716 effect can be observed and of the spatial representativeness of both observations and LES  
 717 simulations. This will also be investigated in a future study.

718 This paper highlights the important role of snow melt and rain evaporation in de-  
 719 pleting the water vapor in case of large-scale ascent. These processes are expected to be  
 720 even stronger in stratiform regions of meso-scale systems, where all the rain arises from  
 721 the widespread melting of snow near the melting level, and where the rain evaporation  
 722 is boosted by the meso-scale downdraft that dries the lower troposphere (Houze, 1977).  
 723 This may explain why observations show that stratiform regions are often more depleted  
 724 than convective regions in squall lines (Risi et al., 2010; Tremoy et al., 2014), and why  
 725 the amount effect is stronger where the fraction of stratiform clouds is larger (Kurita,  
 726 2013; Aggarwal et al., 2016; Sengupta et al., 2020). To check this hypothesis, we plan

727 to analyze in a future study the dependence of water vapor isotopic profiles to large-scale  
 728 circulation in LES with different convective organizations, such as squall lines (Robe &  
 729 Emanuel, 2001; C. Muller, 2013) or tropical cyclones (M. Khairoutdinov & Emanuel, 2013;  
 730 C. J. Muller & Romps, 2018).

731 Finally, this study highlights the key role of both microphysical processes (evap-  
 732 oration, snow melt) and macrophysical processes (entrainment) in the amount effect. While  
 733 entrainment is partly resolved by grid-scale motions, LES models rely strongly on mi-  
 734 crophysical and subgrid-scale turbulence parameterizations in representing these processes.  
 735 What is the sensitivity of the amount effect to these parameterizations? These processes  
 736 are even more crudely parameterized in general circulation models (GCMs). How do GCMs  
 737 represent these processes? More generally, what would be the added value of adding iso-  
 738 topic diagnostics when routinely comparing single-column versions of GCMs to LES sim-  
 739 ulations? This is yet another question that we plan to address in the future.

## 740 Acknowledgments

741 This work was granted access to the HPC resources of IDRIS under the allocation  
 742 2092 made by GENCI. We thank Giuseppe Torri, Jean-Yves Grandpeix, Sandrine Bony,  
 743 Nicolas Rochetin, Olivier Pauluis for discussions. C.M. gratefully acknowledges funding  
 744 from the European Research Council (ERC) under the European Union’s Horizon 2020  
 745 research and innovation programme (Project CLUSTER, grant agreement No 805041).  
 746 The contribution of P.B. was supported by the National Science Foundation under Grant  
 747 No. AGS-1938108. Information on SAM can be found on this web page: <http://rossby.msrc.sunysb.edu/~marat/S>  
 748 All simulation outputs used in this article will be submitted to the PANGEA data repos-  
 749 itory.

## 750 References

- 751 Aggarwal, P. K., Romatschke, U., Araguas-Araguas, L., Belachew, D., Longstaffe,  
 752 F. J., Berg, P., . . . Funk, A. (2016). Proportions of convective and strati-  
 753 form precipitation revealed in water isotope ratios. *Nature Geoscience*, *9*(8),  
 754 624–629, <https://doi.org/10.1038/ngeo2739>.  
 755 Bailey, A., Blossey, P., Noone, D., Nusbaumer, J., & Wood, R. (2017). Detecting  
 756 shifts in tropical moisture imbalances with satellite-derived isotope ratios in  
 757 water vapor. *Journal of Geophysical Research: Atmospheres*, *122*(11), 5763–  
 758 5779.  
 759 Bao, J., Sherwood, S. C., Colin, M., & Dixit, V. (2017). The robust relationship be-  
 760 tween extreme precipitation and convective organization in idealized numerical  
 761 modeling simulations. *Journal of Advances in Modeling Earth Systems*, *9*(6),  
 762 2291–2303.  
 763 Benetti, M., Aloisi, G., Reverdin, G., Risi, C., & Sèze, G. (2015). Importance of  
 764 boundary layer mixing for the isotopic composition of surface vapor over the  
 765 subtropical north atlantic ocean. *Journal of Geophysical Research: Atmo-*  
 766 *spheres*, *120*(6), 2190–2209.  
 767 Blossey, P. N., Kuang, Z., & Romps, D. M. (2010). Isotopic composition  
 768 of water in the tropical tropopause layer in cloud-resolving simulations  
 769 of an idealized tropical circulation. *J. Geophys. Res.*, *115*, D24309,  
 770 doi:10.1029/2010JD014554.  
 771 Bony, S., Risi, C., & Vimeux, F. (2008). Influence of convective processes on the  
 772 isotopic composition ( $\delta^{18}\text{O}$  and  $\delta^2\text{H}$ ) of precipitation and water vapor  
 773 in the Tropics. Part 1: Radiative-convective equilibrium and TOGA-COARE  
 774 simulations. *J. Geophys. Res.*, *113*, D19305, doi:10.1029/2008JD009942.  
 775 Chen, X., Pauluis, O. M., & Zhang, F. (2018). Atmospheric overturning across mul-  
 776 tiple scales of an mjo event during the cindy/dynamo campaign. *Journal of the*

- 777 *Atmospheric Sciences*, 75(2), 381–399.
- 778 Craig, H., & Gordon, L. I. (1965). Deuterium and oxygen-18 variations in the  
779 ocean and marine atmosphere. *Stable Isotope in Oceanographic Studies and*  
780 *Paleotemperatures, Laboratorio di Geologia Nucleate, Pisa, Italy*, 9-130.
- 781 Dansgaard. (1964). Stable isotopes in precipitation. *Tellus*, 16, 436-468.
- 782 Dauhut, T., Chaboureau, J.-P., Mascart, P., & Pauluis, O. (2017). The atmospheric  
783 overturning induced by hector the convector. *Journal of the Atmospheric Sci-*  
784 *ences*, 74(10), 3271–3284.
- 785 Dee, S. G., Nusbaumer, J., Bailey, A., Russell, J. M., Lee, J.-E., Konecky, B., ...  
786 Noone, D. C. (2018). Tracking the strength of the walker circulation with  
787 stable isotopes in water vapor. *Journal of Geophysical Research: Atmospheres*,  
788 123(14), 7254–7270.
- 789 Del Genio, A. D., & Wu, J. (2010). The role of entrainment in the diurnal cycle of  
790 continental convection. *Journal of Climate*, 23(10), 2722–2738.
- 791 De Rooy, W. C., Bechtold, P., Fröhlich, K., Hohenegger, C., Jonker, H., Mironov,  
792 D., ... Yano, J.-I. (2013). Entrainment and detrainment in cumulus con-  
793 vection: An overview. *Quarterly Journal of the Royal Meteorological Society*,  
794 139(670), 1–19.
- 795 Dessler, A. E., & Sherwood, S. C. (2003, December). A model of HDO in the tropi-  
796 cal tropopause layer. *Atmos. Chem. Phys.*, 3, 2173-2181.
- 797 Duan, S. Q., Wright, J. S., & Romps, D. M. (2018). On the utility (or futility) of  
798 using stable water isotopes to constrain the bulk properties of tropical convec-  
799 tion. *Journal of Advances in Modeling Earth Systems*, 10(2), 516–529.
- 800 Field, R. D., Jones, D. B. A., & Brown, D. P. (2010). The effects of post-  
801 condensation exchange on the isotopic composition of water in the atmosphere.  
802 *J. Geophys. Res.*, 115, D24305, doi:10.1029/2010JD014334.
- 803 Field, R. D., Kim, D., LeGrande, A. N., Worden, J., Kelley, M., & Schmidt, G. A.  
804 (2014). Evaluating climate model performance in the tropics with retrievals  
805 of water isotopic composition from Aura TES. *Geophys. Res. Lett.*, DOI:  
806 10.1002/2014GL060572.
- 807 Galewsky, J., & Hurley, J. V. (2010). An advection-condensation model for sub-  
808 tropical water vapor isotopic ratios. *J. Geophys. Res.*, 115 (D16), D16115 ,  
809 doi:10.1029/2009JD013651.
- 810 Galewsky, J., & Rabanus, D. (2016). A stochastic model for diagnosing subtropi-  
811 cal humidity dynamics with stable isotopologues of water vapor. *Journal of the*  
812 *Atmospheric Sciences*, 73(4), 1741–1753.
- 813 Glenn, I. B., & Krueger, S. K. (2014). Downdrafts in the near cloud environment  
814 of deep convective updrafts. *Journal of Advances in Modeling Earth Systems*,  
815 6(1), 1–8.
- 816 Godunov, S. K. (1959). Finite-difference methods for the numerical computations of  
817 equations of gas dynamics. *Math. Sb.*, 7, 271-290.
- 818 Hohenegger, C., & Bretherton, C. S. (2011). Simulating deep convection with a  
819 shallow convection scheme. *Atmospheric Chemistry and Physics*, 11, 10389–  
820 10406.
- 821 Houze, R. A. (1977). Structure and dynamics of a tropical squall line system. *Mon.*  
822 *Wea. Rev.*, 105, 1540-1567.
- 823 Johnson, R. H., Rickenbach, T. M., Rutledge, S. A., Ciesielski, P. E., & Schubert,  
824 W. H. (1999). Trimodal characteristics of tropical convection. *Journal of*  
825 *climate*, 12(8), 2397–2418.
- 826 Khairoutdinov, M., & Emanuel, K. (2013). Rotating radiative-convective equilibrium  
827 simulated by a cloud-resolving model. *Journal of Advances in Modeling Earth*  
828 *Systems*, 5(4), 816–825.
- 829 Khairoutdinov, M. F., & Randall, D. A. (2003). Cloud resolving modeling of the  
830 arm summer 1997 iop: Model formulation, results, uncertainties, and sensitivi-  
831 ties. *Journal of the Atmospheric Sciences*, 60(4), 607–625.

- 832 Kuang, Z., & Bretherton, C. S. (2006). A mass-flux scheme view of a high-resolution  
833 simulation of a transition from shallow to deep cumulus convection. *Journal of*  
834 *the Atmospheric Sciences*, *63*(7), 1895–1909.
- 835 Kurita, N. (2013). Water isotopic variability in response to mesoscale convective  
836 system over the tropical ocean. *Journal of Geophysical Research*, *118*(18), 10-  
837 376.
- 838 Kurita, N., Noone, D., Risi, C., Schmidt, G. A., Yamada, H., & Yoneyama, K.  
839 (2011). Intraseasonal isotopic variation associated with the Madden-Julian  
840 Oscillation. *J. Geophys. Res.*, *116*, D24, D24101, doi:10.1029/2010JD015209.
- 841 Lacour, J.-L., Risi, C., Worden, J., Clerbaux, C., & Coheur, P.-F. (2017). Isotopic  
842 signature of convection’s depth in water vapor as seen from iasi and tes d  
843 observations. *Earth Planet. Sci. Lett.*, *7*, 9645-9663, doi.org/10.5194/acp-17-  
844 9645-2017.
- 845 Lawrence, J. R., Gedzelman, S. D., Dexheimer, D., Cho, H.-K., Carrie, G. D.,  
846 Gasparini, R., . . . Biggerstaff, M. I. (2004, March). Stable isotopic com-  
847 position of water vapor in the tropics. *J. Geophys. Res.*, *109*, D06115,  
848 doi:10.1029/2003JD004046. doi: 10.1029/2003JD004046
- 849 Lee, J.-E., & Fung, I. (2008). "Amount effect" of water isotopes and quantitative  
850 analysis of post-condensation processes. *Hydrological Processes*, *22* (1), 1-8.
- 851 Lee, J.-E., Fung, I., DePaolo, D., & Fennig, C. C. (2007). Analysis of the global  
852 distribution of water isotopes using the NCAR atmospheric general circulation  
853 model. *J. Geophys. Res.*, *112*, D16306, doi:10.1029/2006JD007657.
- 854 Lee, J.-E., Pierrehumbert, R., Swann, A., & Lintner, B. R. (2009). Sensitivity of sta-  
855 ble water isotopic values to convective parameterization schemes. *Geophys. Res.*  
856 *Lett.*, *36*, 3801, doi:10.1029/2009GL040880.
- 857 Merlivat, L., & Jouzel, J. (1979). Global climatic interpretation of the Deuterium-  
858 Oxygen 18 relationship for precipitation. *J. Geophys. Res.*, *84*, 5029-5332.
- 859 Moore, M., Blossey, P., Muhlbauer, A., & Kuang, Z. (2016). Microphysical controls  
860 on the isotopic composition of wintertime orographic precipitation. *Journal of*  
861 *Geophysical Research: Atmospheres*, *121*(12), 7235–7253.
- 862 Moore, M., Kuang, Z., & Blossey, P. N. (2014). A moisture budget per-  
863 spective of the amount effect. *Geophys. Res. Lett.*, *41*, 1329-1335,  
864 doi:10.1002/2013GL058302.
- 865 Mrowiec, A. A., Pauluis, O., Fridlind, A., & Ackerman, A. (2015). Properties of a  
866 mesoscale convective system in the context of an isentropic analysis. *Journal of*  
867 *the Atmospheric Sciences*, *72*(5), 1945–1962.
- 868 Mrowiec, A. A., Pauluis, O. M., & Zhang, F. (2016). Isentropic analysis of a simu-  
869 lated hurricane. *Journal of the Atmospheric Sciences*, *73*(5), 1857–1870.
- 870 Muller, C. (2013). Impact of convective organization on the response of tropical pre-  
871 cipitation extremes to warming. *Journal of climate*, *26*(14), 5028–5043.
- 872 Muller, C. J., & Romps, D. M. (2018). Acceleration of tropical cyclogenesis by  
873 self-aggregation feedbacks. *Proceedings of the National Academy of Sciences*,  
874 201719967.
- 875 Pauluis, O. M., & Mrowiec, A. A. (2013). Isentropic analysis of convective motions.  
876 *Journal of the atmospheric sciences*, *70*(11), 3673–3688.
- 877 Randall, D., Khairoutdinov, M., Arakawa, A., & Grabowski, W. (2003). Breaking  
878 the cloud parameterization deadlock. *Bulletin of the American Meteorological*  
879 *Society*, *84*(11), 1547–1564.
- 880 Risi, C., Bony, S., & Vimeux, F. (2008). Influence of convective processes on the  
881 isotopic composition (O18 and D) of precipitation and water vapor in the  
882 Tropics: Part 2: Physical interpretation of the amount effect. *J. Geophys. Res.*,  
883 *113*, D19306, doi:10.1029/2008JD009943.
- 884 Risi, C., Bony, S., Vimeux, F., Chong, M., & Descroix, L. (2010). Evolution of the  
885 water stable isotopic composition of the rain sampled along Sahelian squall  
886 lines. *Quart. J. Roy. Meteor. Soc.*, *136* (S1), 227 - 242.

- 887 Risi, C., Galewsky, J., Reverdin, G., & Brient, F. (2019). Controls on the wa-  
 888 ter vapor isotopic composition near the surface of tropical oceans and role  
 889 of boundary layer mixing processes. *Atm. Chem. Phys.*, *19*, 12235–12260,  
 890 <https://doi.org/10.5194/acp-19-12235-2019>.
- 891 Risi, C., Muller, C., & N, B. P. (2020). What controls the water vapor isotopic com-  
 892 position near the surface of tropical oceans? results from an analytical model  
 893 constrained by large-eddy simulations. *Journal of Advances in Modeling Earth*  
 894 *Systems*.
- 895 Robe, F. R., & Emanuel, K. A. (2001). The effect of vertical wind shear on  
 896 radiative–convective equilibrium states. *Journal of the atmospheric sciences*,  
 897 *58*(11), 1427–1445.
- 898 Romps, D. M. (2014). An analytical model for tropical relative humidity. *Journal of*  
 899 *Climate*, *27*(19), 7432–7449.
- 900 Rozanski, K., Araguas-Araguas, L., & Gonfiantini, R. (1993). Isotopic patterns in  
 901 modern global precipitation. *Geophys. Monogr. Seri., AGU, Climate Change*  
 902 *in Continental Isotopic records*.
- 903 Schmidt, G., Hoffmann, G., Shindell, D., & Hu, Y. (2005). Modelling atmospheric  
 904 stable water isotopes and the potential for constraining cloud processes and  
 905 stratosphere-troposphere water exchange. *J. Geophys. Res.*, *110*, D21314,  
 906 doi:10.1029/2005JD005790.
- 907 Sengupta, S., Bhattacharya, S. K., Parekh, A., Nimya, S. S., Yoshimura, K., &  
 908 Sarkar, A. (2020). Signatures of monsoon intra-seasonal oscillation and  
 909 stratiform process in rain isotope variability in northern bay of bengal and  
 910 their simulation by isotope enabled general circulation model. *Clim. Dyn.*,  
 911 <https://doi.org/10.1007/s00382-020-05344-w>.
- 912 Sherwood, S. C. (1996). Maintenance of the free tropospheric tropical water va-  
 913 por distribution. part II: simulation of large-scale advection. *J. Clim.*, *11*,  
 914 2919–2934.
- 915 Stevens, B., & Bony, S. (2013). What are climate models missing? *Science*,  
 916 *340*(6136), 1053–1054.
- 917 Thayer-Calder, K., & Randall, D. (2015). A numerical investigation of boundary  
 918 layer quasi-equilibrium. *Geophysical Research Letters*, *42*(2), 550–556.
- 919 Thompson, G., Field, P. R., Rasmussen, R. M., & Hall, W. D. (2008). Explicit fore-  
 920 casts of winter precipitation using an improved bulk microphysics scheme. part  
 921 ii: Implementation of a new snow parameterization. *Monthly Weather Review*,  
 922 *136*(12), 5095–5115.
- 923 Tremoy, G., Vimeux, F., Soumana, S., Souley, I., Risi, C., Cattani, O., . . . Oi, M.  
 924 (2014). Clustering mesoscale convective systems with laser-based water vapor  
 925 delta18O monitoring in Niamey (Niger). *J. Geophys. Res.*, *119*(9), 5079–5103,  
 926 DOI: 10.1002/2013JD020968.
- 927 Wang, Y. J., Cheng, H., Edwards, R. L., An, Z. S., Wu, J. Y., Shen, C. C., & Do-  
 928 rale, J. A. (2001). A high-resolution absolute-dated late Pleistocene Monsoon  
 929 record from Hulu Cave, China. *Science*, *294*(5550), 2345–8.
- 930 Webb, M. J., Lock, A. P., Bretherton, C. S., Bony, S., Cole, J. N., Idelkadi, A., . . .  
 931 others (2015). The impact of parametrized convection on cloud feedback.  
 932 *Philosophical Transactions of the Royal Society A: Mathematical, Physical and*  
 933 *Engineering Sciences*, *373*(2054), 20140414.
- 934 Worden, J., Noone, D., & Bowman, K. (2007). Importance of rain evaporation and  
 935 continental convection in the tropical water cycle. *Nature*, *445*, 528–532.